

# Calculation of $K \rightarrow \pi\pi$ decay amplitudes with improved Wilson fermion action in lattice QCD

N. Ishizuka,<sup>1,2</sup> K.-I. Ishikawa,<sup>3</sup> A. Ukawa,<sup>4</sup> and T. Yoshié<sup>1,2</sup>

<sup>1</sup> *Center for Computational Sciences,  
University of Tsukuba, Tsukuba, Ibaraki 305-8577, Japan*

<sup>2</sup> *Graduate School of Pure and Applied Sciences,  
University of Tsukuba, Tsukuba, Ibaraki 305-8571, Japan*

<sup>3</sup> *Department of Physics, Hiroshima University,  
Higashi-Hiroshima, Hiroshima 739-8526, Japan*

<sup>4</sup> *RIKEN Advanced Institute for Computational Science, Kobe 650-0047, Japan*

(Dated: December 7, 2024)

## Abstract

We present our results for the  $K \rightarrow \pi\pi$  decay amplitudes for both the  $\Delta I = 1/2$  and  $3/2$  channels. Calculations are carried out with  $N_f = 2 + 1$  gauge configurations generated with the Iwasaki gauge action and non-perturbatively  $O(a)$ -improved Wilson fermion action at  $a = 0.091$  fm,  $m_\pi = 280$  MeV and  $m_K = 580$  MeV on a  $32^3 \times 64$  ( $La = 2.9$  fm) lattice. For the quark loops in the penguin and disconnected contributions in the  $I = 0$  channel, the combined hopping parameter expansion and truncated solver method work very well for variance reduction. We obtain, for the first time with a Wilson-type fermion action, that  $\text{Re}A_0 = 60(36) \times 10^{-8}$  GeV and  $\text{Im}A_0 = -67(56) \times 10^{-12}$  GeV for a matching scale  $q^* = 1/a$ . The dependence on the matching scale  $q^*$  for these values is weak.

PACS numbers: 11.15.Ha, 12.38.Gc, 13.25.Es

## I. INTRODUCTION

Calculation of the  $K \rightarrow \pi\pi$  decay amplitudes is very important to quantitatively understand the  $\Delta I = 1/2$  rule in the decay of the neutral  $K$  meson system and to theoretically predict the direct  $CP$  violation parameter ( $\epsilon'/\epsilon$ ) from the Standard Model. A direct lattice QCD calculation of the decay amplitudes for the  $\Delta I = 3/2$  process has been attempted for a long time. Recently the RBC-UKQCD collaboration presents the results at the physical quark mass in Ref. [1] and those in the continuum limit in Ref. [2]. A direct calculation of the decay amplitudes for the  $\Delta I = 1/2$  process has been unsuccessful for a long time, due to large statistical fluctuations from the disconnected diagrams. A first direct calculation was reported by the RBC-UKQCD collaboration in Ref. [3] at a lattice spacing  $a = 0.114$  fm and a pion mass  $m_\pi = 422$  MeV on a  $16^3 \times 32$  lattice with the domain wall fermion action. They also presented a result at a smaller quark mass ( $m_\pi = 330$  MeV) on a  $24^3 \times 64$  lattice with the same fermion action at Lattice 2011 [4]. They attempt direct calculation in the physical kinematics at the physical quark mass, where the pions in the final state have the finite momenta, by imposing  $G$ -parity boundary conditions in the space directions. Their preliminary results are presented in Ref. [5].

An aim of the present article is to report on our calculation of the  $K \rightarrow \pi\pi$  decay amplitudes with the improved Wilson fermion action for both the  $\Delta I = 1/2$  and  $3/2$  processes. That such a calculation is feasible stems from a realization, as shown in the present article, that CPS symmetry [6] and its extensions [7] ensure that mixings with four-fermion operators with wrong chirality are absent even for the Wilson fermion action for the parity odd process in both channels. A mixing to a lower dimension operator does occur, which gives unphysical contributions to the amplitudes on the lattice. However, it can be non-perturbatively subtracted by imposing a renormalization condition [8, 9]. After the subtraction we can obtain the physical decay amplitudes by the renormalization factor having the same structure as for the chiral symmetry preserved case. A potential advantage with the Wilson fermion action over chirally symmetric lattice actions such as the domain wall action is that the computational cost is generally smaller. Hence, with the same amount of computational resources, a statistical improvement may be expected with the lattice calculation of the decay amplitudes, albeit this point has to be verified by actual calculations.

Our calculations are carried out on a subset of gauge configurations previously generated by the PACS-CS collaboration with the Iwasaki gauge action and the non-perturbatively  $O(a)$ -improved Wilson fermion action for  $N_f = 2 + 1$  flavors at  $\beta = 1.9$  on a  $32^3 \times 64$  lattice [10]. The subset corresponds to the hopping parameters  $\kappa_{ud} = 0.13770$  for the up and the down quark and  $\kappa_s = 0.13640$  for the strange quark. We further generate gauge configurations at the same parameters to improve the statistics. The total number of gauge configurations used in the present work is 480. The parameters determined from the hadron spectrum analysis are  $a = 0.091$  fm for the lattice spacing,  $La = 2.91$  fm for the lattice size,  $m_\pi = 275.7(1.5)$  MeV and  $m_K = 579.7(1.3)$  MeV for the pion and the  $K$  masses. We consider the decay of zero momentum  $K$  meson to two zero momentum pions on these configurations. The energy difference between the initial  $K$  meson and the final two-pion

state takes a non-zero value,  $\Delta E = 21(3)$  MeV for the  $I = 2$  channel, and  $36(18)$  MeV for the  $I = 0$  channel on these configurations. In the present work we assume that these mismatches of the energy give only small effects to the decay amplitudes.

This paper is organized as follows. The  $K \rightarrow \pi\pi$  decay amplitudes can be calculated from the product of the  $K \rightarrow \pi\pi$  matrix elements of the  $\Delta S = 1$  four-fermion weak interaction operators and the Wilson coefficient functions for the operator product expansion. In Sec. II these four-fermion operators are introduced and the operator mixing among them for the Wilson fermion action is discussed. In Sec. III we describe the method of calculation used in the present work. The simulation parameters are also given. We present our results in Sec. IV, and compare them with those by the RBC-UKQCD collaboration and the experimental values. Conclusions of the present work are given in Sec. V.

Our calculations have been carried out on the PACS-CS computer and T2K-Tsukuba at University of Tsukuba, the K computer at the RIKEN Advanced Institute for Computational Science, and SR16000 at University of Tokyo. Our preliminary results have been reported at Lattice 2013 and 2014 [11].

## II. $\Delta S = 1$ OPERATORS

### A. $\Delta S = 1$ weak operators in the continuum theory

The effective Hamiltonian of the  $K \rightarrow \pi\pi$  decay in the continuum theory can be written as [12],

$$H = \frac{G_F}{\sqrt{2}} (V_{us}^* V_{ud}) \sum_{i=1}^{10} (z_i(\mu) + \tau y_i(\mu)) Q_i(\mu) , \quad (1)$$

with  $\tau = -(V_{ts}^* V_{td}) / (V_{us}^* V_{ud})$ , and  $z_i(\mu)$  and  $y_i(\mu)$  ( $i = 1, 2, \dots, 10$ ) are the coefficient functions at renormalization scale  $\mu$ . Here we consider the case  $\mu \leq m_c$ , where three light quarks, up, down and strange, are the active quarks in the theory. The ten operators  $Q_i(\mu)$  ( $i = 1, 2, \dots, 10$ ) denote the  $\Delta S = 1$  four-fermion operators renormalized at  $\mu$ , which are given by

$$Q_1 = (\bar{s}d)(\bar{u}u)_{LL} , \quad (2)$$

$$Q_2 = (\bar{s} \times d)(\bar{u} \times u)_{LL} , \quad (3)$$

$$Q_3 = (\bar{s}d) \sum_q (\bar{q}q)_{LL} , \quad (4)$$

$$Q_4 = (\bar{s} \times d) \sum_q (\bar{q} \times q)_{LL} , \quad (5)$$

$$Q_5 = (\bar{s}d) \sum_q (\bar{q}q)_{LR} , \quad (6)$$

$$Q_6 = (\bar{s} \times d) \sum_q (\bar{q} \times q)_{LR} , \quad (7)$$

$$Q_7 = \frac{3}{2} (\bar{s}d) \sum_q e_q (\bar{q}q)_{LR} , \quad (8)$$

$$Q_8 = \frac{3}{2} (\bar{s} \times d) \sum_q e_q (\bar{q} \times q)_{LR} , \quad (9)$$

$$Q_9 = \frac{3}{2} (\bar{s}d) \sum_q e_q (\bar{q}q)_{LL} , \quad (10)$$

$$Q_{10} = \frac{3}{2} (\bar{s} \times d) \sum_q e_q (\bar{q} \times q)_{LL} , \quad (11)$$

where  $(\bar{s}d)(\bar{u}u)_{L,R/L} = (\bar{s}\gamma_\mu(1 - \gamma_5)d)(\bar{u}\gamma_\mu(1 \pm \gamma_5)u)$ , and  $\times$  means the contraction of color indices according to  $(\bar{s} \times d)_L(\bar{u} \times d)_L = \sum_{a,b} (\bar{s}_a d_b)_L (\bar{u}_b d_a)_L$ . The summation for  $q$  is taken for the active quarks ( $q = u, d, s$ ) and the electric charge takes values  $e_u = +2/3$  and  $e_d = e_s = -1/3$ .

In the four-dimensional space-time these operators are not all independent, satisfying the relations :

$$Q_4 = -Q_1 + Q_2 + Q_3 , \quad (12)$$

$$Q_9 = (3Q_1 - Q_3)/2 , \quad (13)$$

$$Q_{10} = (3Q_2 - Q_4)/2 = Q_2 + (Q_1 - Q_3)/2 , \quad (14)$$

due to the Fierz identity. In general dimensions, however, these relations are not valid. Therefor, if we adopt the dimensional regularization for regularization, we should deal with all operators  $Q_i$  for  $i = 1, 2, \dots, 10$  as independent.

## B. Operator mixing for the Wilson fermion action

The matrix elements calculated on the lattice are converted to those in the continuum by the renormalization factor for the operators. The renormalization factor is composed of two parts. The first part is the conversion factor from the operator on the lattice to the operator in the tree order (the renormalization factor for the lattice), and the other part is the factor from the operator in the tree order to the renormalized operator in the continuum (the renormalization factor for the continuum theory). We need to discuss the renormalization factor for the lattice in the case of the Wilson fermion action.

As already mentioned in Sec. II A, the 10 four-fermion operators  $Q_i$  are not independent, and they may be arranged into 7 linearly independent combinations according to the irreducible representation of the flavor  $SU(3)_L \times SU(3)_R$  symmetry group. The 7 operators consist of  $(\mathbf{27}, \mathbf{1}) + 4 \cdot (\mathbf{8}, \mathbf{1}) + 2 \cdot (\mathbf{8}, \mathbf{8})$ , whose components are given by

$$\begin{aligned} (\mathbf{27}, \mathbf{1}) \quad Q'_1 &= 3Q_1 + 2Q_2 - Q_3 , \\ (\mathbf{8}, \mathbf{1}) \quad Q'_2 &= 2Q_1 - 2Q_2 + Q_3 , \\ Q'_3 &= -3Q_1 + 3Q_2 + Q_3 , \end{aligned} \quad (15)$$

$$Q_5, \quad Q_6, \quad (16)$$

$$(8, 8) \quad Q_7, \quad Q_8. \quad (17)$$

The operators  $Q'_{1,2,3}$  are the  $LL$  type fore-fermion operators and  $Q_{5,6,7,8}$  are of  $LR$  type.

If the chiral symmetry is preserved in the regularization, mixings between operators in different representations are forbidden. For the Wilson fermion action, however, chiral symmetry is broken to the vector subgroup,  $SU(3)_L \times SU(3)_R \rightarrow SU(3)_V$ . Hence mixings among different representations is in general allowed, and new operators arise through radiative corrections. However, we show below that such a problem is absent for the parity odd part of the operators in the list of (2)–(11) or of (15)–(17) for the Wilson fermion action employed in the present work.

To investigate the operator mixing, we exploit the full set of unbroken symmetries for the Wilson fermion action, namely flavor  $SU(3)_V$ , parity  $P$ , charge conjugation  $C$  and  $CPS$  which is the symmetry under  $CP$  transformation followed by the exchange of the  $d$  and the  $s$  quarks. All operators in the list (15)–(17) are  $CPS = +1$  operators, but the following operators also have the same quantum numbers including  $CPS$ ,

$$Q_X = (\bar{s}d)(\bar{d}d - \bar{s}s)_{SP+PS}, \quad (18)$$

$$Q_Y = (\bar{s} \times d)(\bar{d} \times d - \bar{s} \times s)_{SP+PS}, \quad (19)$$

where  $(\bar{s}d)(\bar{d}d)_{SP+PS} = (\bar{s}d)_S(\bar{d}d)_P + (\bar{s}d)_P(\bar{d}d)_S$  and  $(\bar{s}d)_S = \bar{s}d$  and  $(\bar{s}d)_P = \bar{s}\gamma_5 d$ . Therefore we have to consider mixings including these operators.

Let us discuss the problem in two steps, first considering mixings through diagrams in which gluons are exchanged between quarks of the four-fermion operators (gluon exchange diagrams), and second through penguin diagrams in which a pair of quarks from the four-fermion operators forms a quark loop.

For the first type of mixings, it was shown in Ref. [7] that the parity odd part of the  $LL$  and  $LR$  type operators, and the  $SP + PS$  type operator do not mix with each other. One can prove this through the use of  $CPS$ ,  $CPS'$  and  $CPS''$  symmetries which holds for the gluon exchange diagrams, where  $S'$  and  $S''$  are defined by

$$S' : (\bar{\psi}_1\psi_2)(\bar{\psi}_3\psi_4) \rightarrow (\bar{\psi}_2\psi_1)(\bar{\psi}_4\psi_3), \quad (20)$$

$$S'' : (\bar{\psi}_1\psi_2)(\bar{\psi}_3\psi_4) \rightarrow (\bar{\psi}_4\psi_3)(\bar{\psi}_2\psi_1). \quad (21)$$

The parity odd part of the  $LL$  and  $LR$  type operators in (15)–(17), which are of  $-VA - AV$  and  $VA - AV$  type, and that of  $Q_{X,Y}$  in (18)–(19), which is of  $SP + PS$  type, are eigenvectors of the  $CPS'$  and  $CPS''$  symmetry with a different set of eigenvalues,

$$\begin{array}{cc} & CPS' \quad CPS'' \\ LL|_{P=-1} = & -VA - AV \quad +1 \quad +1 \\ LR|_{P=-1} = & VA - AV \quad +1 \quad -1 \\ & SP + PS \quad -1 \quad -1 \end{array} \quad (22)$$

Therefore,  $Q_{X,Y}$  (the  $SP + PS$  type) do not mix with the operators (15)–(17) (the  $LL$  and the  $LR$  type).

Furthermore, the operators  $Q_{7,8} \in (\mathbf{8}, \mathbf{8})$  (the  $LR$  type) do not mix with the  $LL$  type operators ( $Q'_{1,2,3} \in (\mathbf{27}, \mathbf{1}), (\mathbf{8}, \mathbf{1})$ ), or with  $Q_{5,6} \in (\mathbf{8}, \mathbf{1})$  (the  $LR$  type) because the gluon exchange diagrams do not change the flavor structure.

In addition, the mixing between the  $(\mathbf{27}, \mathbf{1})$  and  $(\mathbf{8}, \mathbf{1})$  representations is forbidden by the flavor  $SU(3)_V$  symmetry. To sum up, the renormalization factor for the gluon exchange diagrams has the same structure as for the chiral symmetry preserved case.

Next we investigate the possibility of unwanted mixings through the penguin diagrams. In the penguin diagrams for  $Q_{7,8} \in (\mathbf{8}, \mathbf{8})$ , a cancellation of the quark loop at the weak operator occurs between the  $d$  quark and the  $s$  quark contributions. Since this means that the renormalization factor coming from the penguin diagram is proportional to the quark mass difference  $(m_d - m_s)$ , mixings to four-fermion operators are absent due to the dimensional reason. In addition, the operator arising from the penguin diagrams should have the flavor structure  $(\bar{s}d)(\bar{u}u + \bar{d}d + \bar{s}s)$ , which is different from that of  $Q_{7,8}$ . Thus operator mixings from  $Q_{7,8} \in (\mathbf{8}, \mathbf{8})$  to the other representations and their reverse are absent. These statements also hold for  $Q_{X,Y}$  in (18)–(19) for the same reason, and the operators  $Q_{X,Y}$  are fully isolated in the theory. Further the mixing between the  $(\mathbf{27}, \mathbf{1})$  and  $(\mathbf{8}, \mathbf{1})$  representations in the penguin diagrams is forbidden by the flavor  $SU(3)_V$  symmetry. This concludes the proof on the absence of unwanted mixings among parity-odd part of dimension 6 operators.

Up to now, we have shown that the renormalization factor for the parity odd part of the four-fermion operators in (15)–(17) have the same structure as that in the chiral symmetry preserved case. Here we consider the mixing to lower dimensional operators. From  $CPS$  symmetry and the equation of motion of the quark, there is only one operator with the dimension less than 6, which is

$$Q_P = (m_d - m_s) \cdot P = (m_d - m_s) \cdot \bar{s} \gamma_5 d . \quad (23)$$

This operator also appears in the continuum, but does not yield a non-vanishing contribution to the physical decay amplitudes, since it is a total derivative operator. However, this is not valid for the Wilson fermion action due to chiral symmetry breaking by the Wilson term, and the operator (23) does give a non-zero unphysical contribution to the amplitudes on the lattice. This contribution should be subtracted non-perturbatively, because the mixing coefficient includes a power divergence due to the lattice cutoff growing as  $1/a^2$ . In the present work we subtract it by imposing the following condition [8, 9],

$$\langle 0 | \bar{Q}_i | K \rangle = \langle 0 | Q_i - \alpha_i \cdot P | K \rangle = 0 , \quad (24)$$

for each operator  $Q_i$  in (2)–(6). The subtracted operators  $\bar{Q}_i$  are renormalized by the renormalization factor having the same structure as in the chiral symmetry preserved case.

Here we mention an ambiguity in the subtraction procedure. Instead of strictly demanding the subtraction condition (24), we can choose a different subtracted operator,  $\bar{Q}'_i = \bar{Q}_i + \beta_i \cdot Q_P$ , where  $\beta_i$  is a finite constant depending on the quark masses. The constants do not include the power divergence, and they vanish in the chiral limit. In general, such a finite ambiguity seems to remain in final results of the decay amplitude for finite

quark masses, as pointed out in Ref. [9]. Our case, however, is not a such case for the following reason. The operator  $Q_P$  can be written as  $Q_P = (m_d - m_s)/(m_d + m_s) \cdot (\partial_\mu A_\mu - a\overline{X}_A)$  from the PCAC relation for the Wilson fermion action, where  $A_\mu$  is the renormalized axial vector current and  $\overline{X}_A$  is the dimension 5 operator whose matrix element vanishes in the continuum limit. Thus, a  $\beta_i \cdot Q_P$  term yields a contribution of form  $\Delta p \cdot C - \langle \pi\pi | a\overline{X}_A | K \rangle \cdot D$  to the decay amplitude with finite constants  $C$  and  $D$ , where  $\Delta p$  is the momentum difference between the initial and the final state. These contributions do not include any power divergent parts. Thus, by taking  $\Delta p \rightarrow 0$  and the continuum limit, we can safely estimate the physical value of the decay amplitudes without suffering from the ambiguity.

### III. METHOD

#### A. Simulation parameters

Our calculations are carried out on a subset of gauge configurations previously generated by PACS-CS collaboration with the Iwasaki gauge action and non-perturbatively  $O(a)$ -improved Wilson fermion action at  $\beta = 1.9$  on a  $32^3 \times 64$  lattice [10]. The subset corresponds to the hopping parameters  $\kappa_{ud} = 0.13770$  for the up and the down quark and  $\kappa_s = 0.13640$  for the strange quark. In order to improve the statistics we further generate gauge configurations by two runs of the simulation. The first run uses the same algorithm as employed at the same parameters in Ref. [10]. The trajectory length is  $\tau = 1/4$  and the dead/alive link method with random parallel translation is used. The length of MD time, *i.e.*, the number of trajectories multiplied by the trajectory length  $\tau$ , of this run is 6,000 units as compared to 2,000 for the original run of Ref. [10]. The second run does not use the dead/alive link method. All links are active, the trajectory length equals  $\tau = 1$ , and the length of run is also 6,000 MD time units. We measure hadron Green's functions and the decay amplitudes at every 25 MD time units for both runs. The total length of the run is 12,000 MD time units and the total number of gauge configurations employed for the measurement is 480.

We estimate statistical errors by the jackknife method with bins of 10 configurations (250 MD time units). The parameters determined from the spectrum analysis are  $a = 0.091$  fm for lattice spacing,  $La = 2.91$  fm for spatial lattice size, and  $m_\pi = 275.7(1.5)$  MeV and  $m_K = 579.7(1.3)$  MeV for the pion and the  $K$  meson masses.

In the present work we consider the decay of a zero-momentum  $K$  meson to two zero-momentum pions, assuming that the violation of energy conservation gives only small effects to the decay amplitudes. The energy difference between the initial  $K$  meson and the final two-pion state is  $\Delta E \equiv m_K - E_{\pi\pi}^I = 21(3)$  MeV for  $I = 2$  and  $36(18)$  MeV for  $I = 0$  on our configurations as shown in the following section.

## B. Time correlation function for $K \rightarrow \pi\pi$

We extract the matrix element  $\langle K | \bar{Q}_i | \pi\pi; I \rangle$  from the time correlation function for the  $K \rightarrow \pi\pi$  process,

$$G_i^I(t) = \frac{1}{T} \sum_{\delta=0}^{T-1} \langle 0 | W_{K^0}(t_K + \delta) \bar{Q}_i(t + \delta) W_{\pi\pi}^I(t_\pi + \delta, t_\pi + 1 + \delta) | 0 \rangle . \quad (25)$$

Let us describe various features of this definition one by one. Firstly,  $\bar{Q}_i(t)$  is the subtracted weak operator at the time slice  $t$  defined by

$$\bar{Q}_i(t) = \sum_{\mathbf{x}} \bar{Q}_i(\mathbf{x}, t) , \quad (26)$$

with the subtracted operator  $\bar{Q}_i(\mathbf{x}, t)$  at the space-time position  $(\mathbf{x}, t)$  defined in (24).

Secondly, the operator  $W_{K^0}(t)$  is the wall source for the  $K^0$  meson at the time slice  $t$ ,

$$W_{K^0}(t) = -\bar{W}_d(t) \gamma_5 W_s(t) , \quad (27)$$

with the wall source for the quark  $q = u, d, s$ ,

$$W_q(t) = \sum_{\mathbf{x}} q(\mathbf{x}, t) , \quad (28)$$

$$\bar{W}_q(t) = \sum_{\mathbf{x}} \bar{q}(\mathbf{x}, t) . \quad (29)$$

We adopt  $K^0 = -\bar{d}\gamma_5 s$  as the neutral  $K$  meson operator, so our correlation function has an extra minus from the usual convention.

Thirdly, the operator  $W_{\pi\pi}^I(t_1, t_2)$  in (25) is the wall source for the two-pion state with the iso-spin  $I$ , which is defined by

$$W_{\pi\pi}^{I=2}(t_1, t_2) = \left[ \left( W_{\pi^0}(t_1) W_{\pi^0}(t_2) + W_{\pi^+}(t_1) W_{\pi^-}(t_2) \right) / \sqrt{3} + (t_1 \leftrightarrow t_2) \right] / 2 , \quad (30)$$

$$W_{\pi\pi}^{I=0}(t_1, t_2) = \left[ \left( -W_{\pi^0}(t_1) W_{\pi^0}(t_2) / \sqrt{2} + \sqrt{2} W_{\pi^+}(t_1) W_{\pi^-}(t_2) \right) / \sqrt{3} + (t_1 \leftrightarrow t_2) \right] / 2 , \quad (31)$$

where  $W_{\pi^i}(t)$  is the wall source for  $\pi^i$  meson at the time slice  $t$ ,

$$W_{\pi^+}(t) = -\bar{W}_d(t) \gamma_5 W_u(t) , \quad (32)$$

$$W_{\pi^0}(t) = \left( \bar{W}_u(t) \gamma_5 W_u(t) - \bar{W}_d(t) W_d(t) \right) / \sqrt{2} , \quad (33)$$

$$W_{\pi^-}(t) = \bar{W}_u(t) \gamma_5 W_d(t) . \quad (34)$$

The wall source of each pion is separated by one lattice unit according to  $t_1 = t_\pi$  and  $t_2 = t_\pi + 1$  in (25) to avoid contamination from Fierz-rearranged terms.

We impose the periodic boundary condition in all directions. The summation over  $\delta$ , where  $T = 64$  denotes the temporal size of the lattice, is taken in (25) to improve the statistics. The time slice of the  $K$  meson is set at  $t_K = 24$  and that of the two-pion at



$t_\pi = 0$ . The gauge configurations are fixed to the Coulomb gauge at the time slice of the wall source  $t_K + \delta$ ,  $t_1 + \delta$  and  $t_2 + \delta$  for each  $\delta$ .

The mixing coefficient of the lower dimensional operator  $\alpha_i$  in (24) is obtained from the following ratio of the time correlation function,

$$\alpha_i = \sum_{\delta_1=0}^{T-1} \langle 0 | W_{K^0}(t_K + \delta_1) Q_i(t + \delta_1) | 0 \rangle / \sum_{\delta_2=0}^{T-1} \langle 0 | W_{K^0}(t_K + \delta_2) P(t + \delta_2) | 0 \rangle , \quad (35)$$

in the large  $t_K - t$  region, where  $P(t) = \sum_{\mathbf{x}} P(\mathbf{x}, t)$ .

### C. Quark contractions for $K \rightarrow \pi\pi$ and $K \rightarrow 0$

In Fig. 1 we list all of the possible quark contractions for the  $K \rightarrow \pi\pi$  time correlation function  $G_i^I(t)$  in (25). Again there are a number of features, so let us describe them one by one.

1. Time runs from right to left in the diagrams.
2. There are four types of contractions labeled I, II, III and IV.
3. The diagrams show the quark contractions for the four-fermion operator

$$Q = \sum_{a,b,c,d} (\bar{\psi}_a^1 \Gamma_1 \psi_b^2) (\bar{\psi}_c^3 \Gamma_2 \psi_d^4) T_{abcd} , \quad (36)$$

with the color indices  $a, b, c, d$ , where the spin matrix  $\Gamma_{1,2}$  and the color matrix  $T_{abcd}$  are given, depending on the operator  $Q_i$ , as

$$\Gamma_1 = \gamma_\mu(1 - \gamma_5) , \quad \Gamma_2 = \gamma_\mu(1 - \gamma_5) \quad \text{for } Q_{1,2,3,4,9,10} , \quad (37)$$

$$\Gamma_1 = \gamma_\mu(1 - \gamma_5) , \quad \Gamma_2 = \gamma_\mu(1 + \gamma_5) \quad \text{for } Q_{5,6,7,8} , \quad (38)$$

$$T_{abcd} = \delta_{ab}\delta_{cd} \quad \text{for } Q_{1,3,5,7,9} , \quad (39)$$

$$T_{abcd} = \delta_{ad}\delta_{cb} \quad \text{for } Q_{2,4,6,8,10} . \quad (40)$$

4. In the diagrams, unmarked line segments represent quark propagators for the  $u$  or the  $d$  quark, while those marked by 's' are for the strange quark. The filled circles stand for the wall sources for the  $K$  meson or pions. The open circles refer to the matrices  $\Gamma_1$  or  $\Gamma_2$ . The trace for the spin is taken along closed quark lines.
5. The subscript 1 and 2 attached to the four contraction types I though IV refers to the number of the trace for the spin.
6. The superscript 's' for the contractions  $\text{III}_{1,2}$  and  $\text{IV}_{1,2}$  means that the quark loop at the weak operator is for the strange quark.
7. It should be noted that the location of  $\Gamma_1$  and  $\Gamma_2$  for the contraction  $\text{III}_1^s$  and  $\text{IV}_1^s$  are switched from those for  $\text{III}_1$  and  $\text{IV}_1$ .

8. For the contraction  $IV_i$  and  $IV_i^s$  with  $i = 1, 2$  the contribution of the vacuum diagram,  $\langle 0|K(t_K)Q_i(t)|0\rangle\langle 0|W_{\pi\pi}^I(t_\pi, t_\pi + 1)|0\rangle$ , should be subtracted.

Let us write down some explicit examples. For the contraction  $I_2$ , we have,

$$I_2 = \left[ \sum_{a,b,c,d} \sum_{\mathbf{x}} \text{Tr}(W_d(\mathbf{x}, t; t_2) \gamma_5 W_d(t_2; \mathbf{x}, t) \Gamma_2)_{dc} \right. \\ \left. \times \text{Tr}(W_d(\mathbf{x}, t; t_1) \gamma_5 W_d(t_1; t_K) \gamma_5 W_s(t_K; \mathbf{x}, t) \Gamma_1)_{ba} \cdot T_{abcd} + (t_1 \leftrightarrow t_2) \right] / 2, \quad (41)$$

with  $t_1 = t_\pi$  and  $t_2 = t_\pi + 1$ , where the trace is taken for the spin. The three types of  $W_q$  ( $q = d, s$ ) in (41) are the wall source propagators for the quark  $q$  defined by

$$W_q(\mathbf{x}, t; t_0) = \sum_{\mathbf{y}} Q_q(\mathbf{x}, t; \mathbf{y}, t_0), \quad (42)$$

$$W_q(t_0; \mathbf{x}, t) = \sum_{\mathbf{y}} Q_q(\mathbf{y}, t_0; \mathbf{x}, t) = \gamma_5 W_q(\mathbf{x}, t; t_0)^\dagger \gamma_5, \quad (43)$$

$$W_q(t; t_0) = \sum_{\mathbf{x}} W_q(\mathbf{x}, t; t_0), \quad (44)$$

with the quark propagator  $Q_q(\mathbf{x}, t; \mathbf{y}, t_0)$ . Similarly, the contraction  $I_1$  is given by

$$I_1 = \left[ \sum_{a,b,c,d} \sum_{\mathbf{x}} \text{Tr} \left[ (W_d(\mathbf{x}, t; t_2) \gamma_5 W_d(t_2; \mathbf{x}, t) \Gamma_2)_{bc} \right. \right. \\ \left. \left. \times (W_d(\mathbf{x}, t; t_1) \gamma_5 W_d(t_1; t_K) \gamma_5 W_s(t_K; \mathbf{x}, t) \Gamma_1)_{da} \right] \cdot T_{abcd} + (t_1 \leftrightarrow t_2) \right] / 2, \quad (45)$$

where the trace is taken for the spin.

The contraction  $II_2$  is given by

$$II_2 = \left[ \sum_{a,b,c,d} \sum_{\mathbf{x}} \text{Tr}(W_d(\mathbf{x}, t; t_2) \gamma_5 W_d(t_2; t_1) \gamma_5 W_d(t_1; \mathbf{x}, t) \Gamma_2)_{dc} \right. \\ \left. \times \text{Tr}(W_d(\mathbf{x}, t; t_K) \gamma_5 W_s(t_K; \mathbf{x}, t) \Gamma_1)_{ba} \cdot T_{abcd} + (t_1 \leftrightarrow t_2) \right] / 2, \quad (46)$$

and the contraction  $II_1$  is given by

$$II_1 = \left[ \sum_{a,b,c,d} \sum_{\mathbf{x}} \text{Tr} \left[ (W_d(\mathbf{x}, t; t_2) \gamma_5 W_d(t_2; t_1) \gamma_5 W_d(t_1; \mathbf{x}, t) \Gamma_2)_{bc} \right. \right. \\ \left. \left. \times (W_d(\mathbf{x}, t; t_K) \gamma_5 W_s(t_K; \mathbf{x}, t) \Gamma_1)_{da} \right] \cdot T_{abcd} + (t_1 \leftrightarrow t_2) \right] / 2. \quad (47)$$

The contraction  $III_2$  is given by

$$III_2 = \left[ \sum_{a,b,c,d} \sum_{\mathbf{x}} \text{Tr}(W_d(\mathbf{x}, t; t_2) \gamma_5 W_d(t_2; t_1) \gamma_5 W_d(t_1; t_K) \gamma_5 W_s(t_K; \mathbf{x}, t) \Gamma_1)_{ba} \right. \\ \left. \times \text{Tr}(Q_d(\mathbf{x}, t; \mathbf{x}, t) \Gamma_2)_{dc} \cdot T_{abcd} + (t_1 \leftrightarrow t_2) \right] / 2, \quad (48)$$

where the quark loop for the  $d$  quark  $Q_d(\mathbf{x}, t; \mathbf{x}, t)$  is calculated by the the stochastic method, whose detail is discussed in the next section. The contraction  $\text{III}_2^s$  is obtained by changing  $Q_d(\mathbf{x}, t; \mathbf{x}, t)$  to the quark loop for the  $s$  quark  $Q_s(\mathbf{x}, t; \mathbf{x}, t)$ .

Having constructed various quark contractions, we can build the  $K \rightarrow \pi\pi$  time correlation function  $G_i^I(t)$  for the operators  $Q_i$  in the iso-spin channel  $I$  in the following way. For the  $I = 2$  case, we have

$$G_1^{I=2} = \frac{\sqrt{3}}{3} (\text{I}_2 - \text{I}_1) = G_2^{I=2} = \frac{2}{3} G_9^{I=2} = \frac{2}{3} G_{10}^{I=2} , \quad (49)$$

$$G_7^{I=2} = \frac{\sqrt{3}}{2} (\text{I}_2 - \text{I}_1) , \quad (50)$$

$$G_8^{I=2} = \frac{\sqrt{3}}{2} (\text{I}_2 - \text{I}_1) , \quad (51)$$

where  $\Gamma_{1,2}$  and  $T_{abcd}$  in each contractions should be chosen according to (37)–(40) for each operator. The relation among different operators (49) follows from the Fierz identity.

The formulæ for the  $I = 0$  channel are given as follows:

$$\begin{aligned} \text{for } (\bar{s}d)(\bar{u}u) &= Q_{1,2} \\ G^{I=0} &= \sqrt{\frac{1}{6}} (-\text{I}_2 - 2 \cdot \text{I}_1 + 3 \cdot \text{II}_2 + 3 \cdot \text{T}_2) , \end{aligned} \quad (52)$$

$$\begin{aligned} \text{for } (\bar{s}d)(\bar{u}u + \bar{d}d + \bar{s}s) &= Q_{3,4,5,6} \\ G^{I=0} &= \sqrt{\frac{3}{2}} (-\text{I}_2 + 2 \cdot \text{II}_2 - \text{II}_1 + 2 \cdot \text{T}_2 - \text{T}_1 + \text{T}_2^s - \text{T}_1^s) , \end{aligned} \quad (53)$$

$$\begin{aligned} \text{for } (\bar{s}d)(\bar{u}u - \bar{d}d/2 - \bar{s}s/2) &= Q_{7,8,9,10} \\ G^{I=0} &= \sqrt{\frac{3}{8}} (-\text{I}_2 - \text{I}_1 + \text{II}_2 + \text{II}_1 + \text{T}_2 + \text{T}_1 - \text{T}_2^s + \text{T}_1^s) , \end{aligned} \quad (54)$$

with  $\text{T}_i = \text{III}_i - \text{IV}_i$  and  $\text{T}_i^s = \text{III}_i^s - \text{IV}_i^s$  ( $i = 1, 2$ ), where  $\Gamma_{1,2}$  and  $T_{abcd}$  in each contractions should be chosen according to (37)–(40) for each operator.

We now turn to the quark contractions needed to subtract the contribution of the lower dimension operator  $P = \bar{s}\gamma_5 d$ . In Fig. 2 we list all of the possible quark contractions for the  $K$ -to-vacuum time correlation function  $G_{K \rightarrow 0} = \langle 0 | W_{K^0}(t_K) Q_i(t) | 0 \rangle$  in (35). The notations are the same as for Fig. 1. The contractions for the operators  $Q_i$  are given by

$$\begin{aligned} \text{for } (\bar{s}d)(\bar{u}u) &= Q_{1,2} \\ G_{K \rightarrow 0} &= -\text{V}_2 , \end{aligned} \quad (55)$$

$$\begin{aligned} \text{for } (\bar{s}d)(\bar{u}u + \bar{d}d + \bar{s}s) &= Q_{3,4,5,6} \\ G_{K \rightarrow 0} &= -2 \cdot \text{V}_2 + \text{V}_1 - \text{V}_2^s + \text{V}_1^s , \end{aligned} \quad (56)$$

$$\begin{aligned} \text{for } (\bar{s}d)(\bar{u}u - \bar{d}d/2 - \bar{s}s/2) &= Q_{7,8,9,10} \\ G_{K \rightarrow 0} &= (-\text{V}_2 - \text{V}_1 + \text{V}_2^s - \text{V}_1^s)/2 , \end{aligned} \quad (57)$$

where  $\Gamma_{1,2}$  and  $T_{abcd}$  in each contractions should be chosen according to (37)–(40) for each operator. We can obtain the mixing coefficient of the lower dimensional operator  $\alpha_i$  in (24) by dividing these by the time correlation function  $\langle 0 | W_{K^0}(t_K) P(t) | 0 \rangle$  as (35).

The  $K \rightarrow \pi\pi$  time correlation function for the operator  $P = \bar{s}\gamma_5 d$  is calculated by

$$G_P^I(t) = \frac{1}{T} \sum_{\delta=0}^{T-1} \langle 0 | W_{K^0}(t_K + \delta) P(t + \delta) W_{\pi\pi}^I(t_\pi + \delta, t_\pi + 1 + \delta) | 0 \rangle = -\frac{3}{\sqrt{6}} T_P, \quad (58)$$

where  $T_P = \text{III}_P - \text{IV}_P$ , and the contractions  $\text{III}_P$  and  $\text{IV}_P$  are shown in Fig. 3. For the contractions  $\text{IV}_P$  the contribution of the vacuum diagram  $\langle 0 | K(t_K) P(t) | 0 \rangle \langle 0 | W_{\pi\pi}^I(t_\pi, t_\pi + 1) | 0 \rangle$  is supposed to be subtracted.

The  $K \rightarrow \pi\pi$  time correlation for the subtracted operator  $\bar{Q}_i = Q_i - \alpha_i \cdot P$  is given by subtracting the contributions of  $\alpha_i \cdot P$  from those of the operator  $Q_i$ . We write these subtractions as

$$\text{III} \rightarrow \text{III} - \alpha_i \frac{-3}{\sqrt{6}} \text{III}_P, \quad (59)$$

$$\text{IV} \rightarrow \text{IV} - \alpha_i \frac{-3}{\sqrt{6}} \text{IV}_P, \quad (60)$$

dividing into the connected (III and  $\text{III}_P$ ) and the disconnected contractions (IV and  $\text{IV}_P$ ), where III means the total contribution from the two contractions  $\text{III}_i$  and  $\text{III}_i^s$  for  $i = 1, 2$ , and similarly for IV.

#### D. Calculation of quark loop

The quark loop at the weak operator  $Q(x, x)$ , *i.e.*, the quark propagator starting from the position of the weak operator and ending at the same position, appears in the quark contractions III, IV,  $\text{III}^s$  and  $\text{IV}^s$  for the  $K \rightarrow \pi\pi$  process, and V and  $\text{V}^s$  for the  $K \rightarrow 0$  process, as shown in the previous subsection. We calculate them by the stochastic method with the hopping parameter expansion technique (HPE) and the truncated solver method (TSM) proposed in Ref. [13].

The Wilson fermion action can be written as

$$S^W = \bar{\psi} W \psi = \bar{\psi} (M - D) \psi = \bar{\psi} M (1 - \bar{D}) \psi, \quad (61)$$

where  $\bar{D} = M^{-1}D$  and

$$(M\psi)(x) = (1 - \kappa C_{SW}(\sigma \cdot F(x))/2) \psi(x), \quad (62)$$

$$(D\psi)(x) = \left( \sum_{\mu} (D_{\mu}^+ + D_{\mu}^-) \psi \right) (x), \quad (63)$$

$$(D_{\mu}^+ \psi)(x) = \kappa (1 - \gamma_{\mu}) U_{\mu}(x) \psi(x + \mu), \quad (64)$$

$$(D_{\mu}^- \psi)(x) = \kappa (1 + \gamma_{\mu}) U_{\mu}^{\dagger}(x - \mu) \psi(x - \mu). \quad (65)$$

The quark field of the Wilson fermion  $\psi$  is related to that in the continuum theory  $\psi^c$  by  $\psi^c = \sqrt{2\kappa} \cdot \psi$  in the tree order. From (61) the quark propagator  $Q$  can be written by a

hopping parameter expansion form as

$$Q = W^{-1} = \sum_{n=0}^{\infty} \bar{D}^n M^{-1} = \sum_{n=0}^{k-1} \bar{D}^n M^{-1} + \bar{D}^k W^{-1} \quad (66)$$

for any integer value of  $k$ . We use this expansion to calculate the quark loop  $Q(x, x)$  at the weak operator. In this case, the terms with odd power of  $\bar{D}$  do not contribute, thus

$$Q(x, x) = (M^{-1} + \bar{D}^2 M^{-1} + \bar{D}^4 W^{-1})(x, x) , \quad (67)$$

for  $k = 4$ . We can replace  $\bar{D}^2$  term by

$$\bar{D}_{2L} = \sum_{\mu} (\bar{D}_{\mu}^+ \bar{D}_{\mu}^- + \bar{D}_{\mu}^- \bar{D}_{\mu}^+) , \quad (68)$$

with  $\bar{D}_{\mu}^{\pm} = M^{-1} D_{\mu}^{\pm}$ . Using these expressions, we calculate the quark loop by the stochastic method according to

$$Q(\mathbf{x}, t; \mathbf{x}, t) = \frac{1}{N_R} \sum_{i=1}^{N_R} \xi_i^*(\mathbf{x}, t) S_i(\mathbf{x}, t) . \quad (69)$$

The function  $S_i(\mathbf{x}, t)$  is defined by

$$S_i(\mathbf{x}, t) = \sum_{\mathbf{y}} (M^{-1} + \bar{D}_{2L} M^{-1} + \bar{D}^4 W^{-1})(\mathbf{x}, t; \mathbf{y}, t) \xi_i(\mathbf{y}, t) , \quad (70)$$

where we introduce an  $U(1)$  noise  $\xi_i(\mathbf{x}, t)$  which satisfies

$$\delta^3(\mathbf{x} - \mathbf{y}) = \frac{1}{N_R} \sum_{i=1}^{N_R} \xi_i^*(\mathbf{x}, t) \xi_i(\mathbf{y}, t) , \quad (71)$$

for  $N_R \rightarrow \infty$ . The effect of HPE for the quark loop is to remove the  $\bar{D}$  and  $\bar{D}^3$  terms in (70) explicitly which make only statistical noise. We find that HPE reduces the statistical error of the decay amplitudes to about 50% compared with the normal stochastic method.

We also implement the truncated solver method (TSM) for (69) by

$$Q(\mathbf{x}, t; \mathbf{x}, t) = \frac{1}{N_R} \sum_{i=1}^{N_R} \xi_i^*(\mathbf{x}, t) [S_i(\mathbf{x}, t) - S_i^T(\mathbf{x}, t)] + \frac{1}{N_T} \sum_{i=N_R+1}^{N_R+N_T} \xi_i^*(\mathbf{x}, t) S_i^T(\mathbf{x}, t) , \quad (72)$$

where  $S_i^T(\mathbf{x}, t)$  is a value given with the quark propagator  $W^{-1}$  in (70) calculated with a loose stopping condition, and  $S_i(\mathbf{x}, t)$  is that with a stringent condition. We set  $N_T = 5$  and the stopping condition  $R \equiv |Wx - \xi|/|\xi| < 1.2 \times 10^{-6}$  with  $x$  denoting the iterative solution of  $Wx = \xi$  for  $S_i^T(\mathbf{x}, t)$ , and  $N_R = 1$  and  $R < 10^{-14}$  for  $S_i(\mathbf{x}, t)$  in the present work. The numerical cost of TSM (72) is about twice of that without TSM (69) with  $N_R = 1$ .

### E. Time correlation function for $\pi\pi \rightarrow \pi\pi$

We calculate two types of time correlation functions for  $\pi\pi \rightarrow \pi\pi$  to obtain the normalization factors which are needed to extract the matrix elements  $\langle K|\bar{Q}_i|\pi\pi; I \rangle$  from the time correlation function  $G_i^I(t)$  in (25). These are point-wall and wall-wall time correlation functions, which are defined by

$$G_{PW}^I(t) = \frac{1}{T} \sum_{\delta=0}^{T-1} \langle 0 | (\pi\pi)^I(t+\delta) W_{\pi\pi}^I(t_\pi + \delta, t_\pi + 1 + \delta) | 0 \rangle , \quad (73)$$

$$G_{WW}^I(t) = \frac{1}{T} \sum_{\delta=0}^{T-1} \langle 0 | W_{\pi\pi}^I(t+\delta, t+1+\delta) W_{\pi\pi}^I(t_\pi + \delta, t_\pi + 1 + \delta) | 0 \rangle , \quad (74)$$

where  $(\pi\pi)^I(t)$  is the operator for the two-pion system with the iso-spin  $I$ ,

$$(\pi\pi)^{I=2}(t) = \sum_{\mathbf{x}, \mathbf{y}} \left( \pi^0(\mathbf{x}, t) \pi^0(\mathbf{y}, t) + \pi^+(\mathbf{x}, t) \pi^-(\mathbf{y}, t) \right) / \sqrt{3} , \quad (75)$$

$$(\pi\pi)^{I=0}(t) = \sum_{\mathbf{x}, \mathbf{y}} \left( -\pi^0(\mathbf{x}, t) \pi^0(\mathbf{y}, t) / \sqrt{2} + \sqrt{2} \pi^+(\mathbf{x}, t) \pi^-(\mathbf{y}, t) \right) / \sqrt{3} , \quad (76)$$

with the operator for  $\pi^i$  meson  $\pi^i(\mathbf{x}, t)$  defined by

$$\pi^+(\mathbf{x}, t) = -\bar{d}(\mathbf{x}, t) \gamma_5 u(\mathbf{x}, t) , \quad (77)$$

$$\pi^0(\mathbf{x}, t) = \left( \bar{u}(\mathbf{x}, t) \gamma_5 u(\mathbf{x}, t) - \bar{d}(\mathbf{x}, t) \gamma_5 d(\mathbf{x}, t) \right) / \sqrt{2} , \quad (78)$$

$$\pi^-(\mathbf{x}, t) = \bar{u}(\mathbf{x}, t) \gamma_5 d(\mathbf{x}, t) . \quad (79)$$

The operator  $W_{\pi\pi}^I(t_1, t_2)$  ( $I = 0, 2$ ) is defined by (30) and (31). In the present work we set  $t_\pi = 0$  in (73) and (74)

In Fig. 4 we list all of the possible quark contractions for the time correlation function for the  $\pi\pi \rightarrow \pi\pi$  processes. Time runs from right to left in the diagrams. There are four types of contractions, D, C, R and V. The filled circles represent the wall source  $W_{\pi^i}$  in (32)-(34) or the point source  $\pi^i$  in (77)-(79) for the pion. For the contraction V the contribution of the vacuum diagram,  $\langle 0 | (\pi\pi)^I(t) | 0 \rangle \langle 0 | W_{\pi\pi}^I(t_\pi, t_\pi + 1) | 0 \rangle$  or  $\langle 0 | W_{\pi\pi}^I(t, t+1) | 0 \rangle \langle 0 | W_{\pi\pi}^I(t_\pi, t_\pi + 1) | 0 \rangle$ , is supposed to be subtracted.

For example, the explicit form for the contraction C for the point-wall time correlation function  $G_{PW}^I(t)$  in (73) is given by

$$\begin{aligned} C = & \left[ \sum_{\mathbf{x}, \mathbf{y}} \text{Tr} ( W_d(t_1; \mathbf{y}, t) \gamma_5 W_d(\mathbf{y}, t; t_2) \gamma_5 W_d(t_2; \mathbf{x}, t) \gamma_5 W_d(\mathbf{x}, t; t_1) \gamma_5 ) \right. \\ & \left. + (t_1 \leftrightarrow t_2) \right] / 2 , \end{aligned} \quad (80)$$

with  $t_1 = t_\pi$  and  $t_2 = t_\pi + 1$ , and that for the wall-wall correlation function  $G_{WW}^I(t)$  in (74) by

$$C = \left[ \text{Tr} ( W_d(t_1; t_4) \gamma_5 W_d(t_4; t_2) \gamma_5 W_d(t_2; t_3) \gamma_5 W_d(t_3; t_1) \gamma_5 ) \right]$$

$$+ (t_1 \leftrightarrow t_2) + (t_3 \leftrightarrow t_4) + (t_1 \leftrightarrow t_2, t_3 \leftrightarrow t_4) \Big] / 4 , \quad (81)$$

with  $t_1 = t_\pi$ ,  $t_2 = t_\pi + 1$ ,  $t_3 = t$ ,  $t_4 = t + 1$ , where the trace is taken for the color and the spin indices. The wall source propagators  $W_d$  are defined by (42)-(44).

For the calculation of the contraction R for the point-wall time correlation function  $G_{PW}^I(t)$  in (73), we use the stochastic method according to

$$\begin{aligned} R = \Big[ \frac{1}{N_R} \sum_{i=1}^{N_R} \sum_{\mathbf{x}, \mathbf{y}} \text{Tr} ( W_d(t_1; t_2) \gamma_5 W_d(t_2; \mathbf{x}, t) \gamma_5 Z_i(\mathbf{x}, t) \xi_i^*(\mathbf{y}, t) \gamma_5 W_d(\mathbf{y}, t; t_1) \gamma_5 ) \\ + (t_1 \leftrightarrow t_2) \Big] / 2 , \end{aligned} \quad (82)$$

with  $t_1 = t_\pi$  and  $t_2 = t_\pi + 1$ , where  $\xi_i(\mathbf{y}, t)$  is an  $U(1)$  noise which satisfies (71), and  $Z_i(\mathbf{x}, t)$  is defined by

$$Z_i(\mathbf{x}, t) = \sum_{\mathbf{y}} W^{-1}(\mathbf{x}, t; \mathbf{y}, t) \xi_i(\mathbf{y}, t) , \quad (83)$$

with the kernel of the Wilson fermion  $W$  in (61). The contraction V is also calculated by using  $Z_i(\mathbf{x}, t)$ . In actual calculations, we find that relaxing the stopping condition to  $|Wx - \xi|/|\xi| < 1.2 \times 10^{-6}$  for the calculation of  $Z_i(\mathbf{x}, t)$  makes only negligible effects to the final result, compared with the statistical error. Thus we adopt this loose stopping condition with  $N_R = 6$  in (82).

The quark contraction for the time correlation function,  $G_{PW}^I(t)$  or  $G_{WW}^I(t)$ , is given by

$$G^{I=2} = D - C , \quad (84)$$

$$G^{I=0} = D + \frac{1}{2} C - 3 R + \frac{3}{2} V . \quad (85)$$

## IV. RESULTS

### A. Time correlation function for $\pi\pi \rightarrow \pi\pi$

Fig. 5 shows the contributions of the four types of contractions, D, C, R, V, for the time correlation function for  $\pi\pi \rightarrow \pi\pi$ , with those for the point-wall function  $G_{PW}^I(t)$  in (73) plotted on the left and those for the wall-wall function  $G_{WW}^I(t)$  in (74) on the right panel. The source operator is placed at  $t_\pi = 0$ . The time correlation functions behave in the large time region as

$$G_{PW}^I(t) = A^I \cdot \left( e^{-E_{\pi\pi}^I t} + e^{-E_{\pi\pi}^I (T-t)} \right) + C^I , \quad (86)$$

$$G_{WW}^I(t) = A_{\pi\pi}^I \cdot \left( e^{-E_{\pi\pi}^I t} + e^{-E_{\pi\pi}^I (T-t)} \right) + D^I , \quad (87)$$

where  $E_{\pi\pi}^I$  is the energy of the two-pion system with the iso-spin  $I$ ,  $A^I$  is a constant whose form is irrelevant, and

$$A_{\pi\pi}^I = \langle 0 | W_{\pi\pi}^I(0, 1) | \pi\pi; I \rangle^2 / \langle \pi\pi; I | \pi\pi; I \rangle . \quad (88)$$

The constant terms  $C^I$  and  $D^I$  in (86) and (87) come from the two pions propagating in the opposite time directions (*i.e.*, around-the-world effect for the two-pion operator).

The effective mass of the point-wall time correlation function  $G_{PW}^I(t)$  is plotted in Fig. 6, where the effective mass  $m_{eff}$  at  $t$  is given by

$$\frac{G_{PW}^I(t+1) - G_{PW}^I(t+4)}{G_{PW}^I(t) - G_{PW}^I(t+3)} = \frac{f(t+1; m_{eff}) - f(t+4; m_{eff})}{f(t; m_{eff}) - f(t+3; m_{eff})} \quad (89)$$

with the function  $f(t; m_{eff}) = \exp(-m_{eff} \cdot t) + \exp(-m_{eff} \cdot (T - t))$ . We find plateaus in the time region  $t \geq 9$  for both  $I = 0$  and  $2$ , albeit admittedly much noisier for  $I = 0$  than for  $I = 2$ . Compared with the value  $2m_\pi$  plotted in blue, the two-pion energy for  $I = 2$  is larger, signifying repulsive interaction of the two-pion system, whereas that for  $I = 0$  is smaller showing attractive interaction.

In the extraction of the matrix elements  $\langle K | \overline{Q}_i | \pi\pi; I \rangle$  from the time correlation function  $G_i^I(t)$  in (25), the values of  $E_{\pi\pi}^I$  and  $A_{\pi\pi}^I$  are needed. Since the statistical error of the point-wall correlation function  $G_{PW}^I(t)$  is smaller than that for the wall-wall function  $G_{WW}^I(t)$ , we first extract the energy  $E_{\pi\pi}^I$  from  $G_{PW}^I(t)$ , and then extract the amplitude  $A_{\pi\pi}^I$  from  $G_{WW}^I(t)$  by fitting to (87) with the determined value of  $E_{\pi\pi}^I$  and regarding  $A_{\pi\pi}^I$  and  $D^I$  as unknown parameters. The results for  $E_{\pi\pi}^I$  and  $A_{\pi\pi}^I$  are

$$\begin{aligned} E_{\pi\pi}^{I=2} &= 0.2567(14) , & A_{\pi\pi}^{I=2} &= 2.513(27) \times 10^{20} , \\ E_{\pi\pi}^{I=0} &= 0.2499(83) , & A_{\pi\pi}^{I=0} &= 2.41(13) \times 10^{20} , \end{aligned} \quad (90)$$

in the lattice unit, where we adopt the fitting range  $t = [9, 32]$  for  $I = 2$  and  $t = [9, 12]$  for  $I = 0$ .

The mass of the pion and the  $K$  meson obtained in the present work are  $m_\pi = 0.12671(71)$  and  $m_K = 0.26641(58)$  in the lattice unit. The energy difference between the initial  $K$  meson and the final two-pion state,  $\Delta E^I = m_K - E_{\pi\pi}^I$ , is  $\Delta E^{I=2} = 0.0097(14)$  (21(3) MeV) and  $\Delta E^{I=0} = 0.0165(83)$  (36(18) MeV). In the present work, we assume that these violations of energy conservation yield only small effects to the results for the  $K \rightarrow \pi\pi$  decay amplitudes.

## B. Time correlation function for $K \rightarrow \pi\pi$ in the $I = 0$ channel

In Fig. 7 we demonstrate the effects of the truncated solver method. The four panels (a)–(d) show the contributions of the contractions III and IV to the time correlation functions for  $\overline{Q}_2$  and  $\overline{Q}_6$  at  $t = 9$ . In each panel, the data at  $x = 0$  shows the result of a stochastic estimate with a stringent stopping condition, while those at  $x = 1, \dots, 6$  are obtained with a loose stopping condition, with an identical noise vector employed for  $x = 0$  and  $x = 1$ . Thus, the difference between the data at  $x = 0$  and  $x = 1$  corresponds to the first term of (72) for  $N_R = 1$ , and the data at  $x = 2, \dots, 6$  ( $N_T = 5, N_T + N_R = 6$ ) correspond to the components of the second term of (72). We find that the first term is negligible compared with the statistical error for all channels. Thus we can neglect it, and estimate the quark



loop contribution by only the second term as

$$Q(\mathbf{x}, t; \mathbf{x}, t) = \frac{1}{N_T + N_R} \sum_{i=1}^{N_T + N_R} \xi_i^*(\mathbf{x}, t) S_i^T(\mathbf{x}, t) . \quad (91)$$

The contribution given by the sum (91) is plotted at  $x = 7$  in each panel. We see that the statistics is significantly improved by increasing the number of random numbers from 1 to 6.

The results for the  $I = 0$   $K \rightarrow \pi\pi$  time correlation function for the operator  $Q_2$  ( $G_2^{I=0}(t)$  in (25)) are plotted in Fig. 8. The time slice of the two-pion is set at  $t_\pi = 0$  and the  $K$  meson at  $t_K = 24$ , while the operator  $Q_i(t)$  runs over the whole time extent as explained before. In the panels (a) and (b), we observe a large cancellation between the contributions from the operator  $Q_2$  and the subtraction term  $\alpha_2 \cdot P$  for both contractions III and IV. In panel (c) we find that the contribution from the contraction IV is similar in magnitude to that from the contraction I. This appears different from the previous work by RBC-UKQCD collaboration with the domain wall fermion action in Refs. [3, 4]. In panel (d) we compare the correlation functions calculated with TSM and without TSM. We find that TSM significantly improves the statistics. The numerical cost of TSM is about twice of that without TSM. Thus TSM is a very efficient method.

The results for  $Q_6$  in the  $I = 0$  channel are plotted in Fig. 9. Here also we find a large cancellation between the contributions of  $Q_6$  and the subtraction  $\alpha_6 \cdot P$  for both contractions III and IV (see panel (a) and (b)). In panel (c) a large cancellation is observed between the contraction I and II, which is not the case for  $\overline{Q}_2$ . An efficiency of TSM is observed also for  $Q_6$  in panel (d).

### C. $K \rightarrow \pi\pi$ matrix elements

In order to extract the  $K \rightarrow \pi\pi$  matrix element we consider an effective matrix element  $M_i^I(t)$ , which behaves as  $M_i^I(t) = M_i^I \equiv \langle K | \overline{Q}_i(\mathbf{0}, 0) | \pi\pi; I \rangle$  in the time region  $t_K \gg t \gg t_\pi$ . It can be constructed from the time correlation function  $G_i^I(t)$  in (25) by

$$M_i^I(t) = G_i^I(t) / \sqrt{A_K A_{\pi\pi}^I} \cdot F^I \cdot e^{m_K(t_K - t) + E_{\pi\pi}^I(t - t_\pi)} \times (-1) . \quad (92)$$

Here, the  $K$  meson mass  $m_K$  and the energy of the two-pion state  $E_{\pi\pi}^I$  are fixed at the values obtained from the correlation function of the  $K$  meson and the  $\pi\pi \rightarrow \pi\pi$ . The factor  $(-1)$  comes from the convention of the  $K^0$  operator in (27). The constant  $A_K = \langle 0 | W_K | K \rangle^2 / \langle K | K \rangle$  is estimated from the wall-wall propagator of the  $K$  meson, with the value  $A_K = 8.949(34) \times 10^9$  in the lattice unit. The constant  $A_{\pi\pi}^I$  is defined by (88) and its value is given by (90). The dimensionless constant  $F^I$  is the Lellouch-Lüscher factor [14] given by

$$\begin{aligned} (F^I)^2 &= \langle K | K \rangle \cdot \langle \pi\pi; I | \pi\pi; I \rangle / V^2 \\ &= (4\pi) \left( \frac{(E_{\pi\pi}^I)^2 m_K}{p^3} \right) \left( p \frac{\partial \delta^I(p)}{\partial p} + q \frac{\partial \phi(q)}{\partial q} \right) , \end{aligned} \quad (93)$$

where  $V$  is the lattice volume  $V = L^3$ ,  $\delta^I(p)$  is the two-pion scattering phase shift for the two-pion system with the iso-spin  $I$  at the scattering momentum  $p^2 = (E_{\pi\pi}^I)^2/4 - m_\pi^2$ , and  $\phi(q)$  is the function defined by

$$\tan \phi(q) = -\pi^{3/2} q / Z_{00}(1; q) , \quad (94)$$

with the spherical zeta function,

$$Z_{00}(s; q) = \frac{1}{\sqrt{4\pi}} \sum_{\mathbf{n} \in \mathbb{Z}^3} (n^2 - q^2)^{-s} , \quad (95)$$

at  $q = p(2\pi/L)$ . In the non-interacting two-pion case, the factor takes the form  $(F^I)^2 \equiv (F|_{\text{free}})^2 = (2m_K V) \cdot (2m_\pi V)^2 / V^2$ .

For the  $I = 0$  channel the statistics in the present work is not sufficient to obtain the scattering phase shift. We therefore use the factor for the non-interacting case, leaving a precise estimation of the factor to studies in the future. For the  $I = 2$  case the phase shift is obtained with a sufficient statistics at the needed momentum. Because the scattering momentum  $p$  takes a small value,  $p = 2.053(97) \times 10^{-2}$  (44.7(2.1) MeV) in our case, the phase shift can be approximated by  $\delta^{I=2}(p) = p(\partial\delta^{I=2}(p)/\partial p) + \mathcal{O}(p^3)$ . We neglect the cubic term, and find  $F^{I=2}/F|_{\text{free}} = 0.9254(62)$ .

Our results for the effective matrix elements for several representative channels are shown in Fig. 10 and Fig. 11 for  $I = 2$ , and in Fig. 12 for  $I = 0$ , where the matrix elements calculated with  $t_K = 22, 24$  and  $26$  are plotted. We find plateaux for the effective matrix elements over the time interval  $t = [9, 12]$  which are independent of the value of  $t_K$ . This means that the around-the-world effect of the two-pion operator is negligible in this time region.

We extract the matrix element  $M_i^I \equiv \langle K | \overline{Q}_i(\mathbf{0}, 0) | \pi\pi; I \rangle$  by a constant fit of the effective amplitude for  $t_K = 24$  in the time interval  $t = [9, 12]$ . Our results for the  $I = 2$  channel (the  $\Delta I = 3/2$  process) are tabulated in the second column in Table I, where the relation among the matrix elements (49) is used. The results for the  $I = 0$  channel (the  $\Delta I = 1/2$  process) are tabulated in the second column in Table II. Here we do not use the operator relations (12)–(14), and treat each of 10 operators as independent.

#### D. $K \rightarrow \pi\pi$ decay amplitudes

The renormalized matrix elements  $\overline{M}_i^I(\mu)$  are obtained from the bare matrix elements on the lattice  $M_j^I$  extracted in the previous section by multiplying with the renormalization factors as

$$\overline{M}_i^I(q^*) = \sum_{j=1}^{10} M_j^I Z_{ji}(q^*a) . \quad (96)$$

The renormalization factors  $Z_{ij}(q^*a)$  for our choice of the fermion and gluon actions have been calculated by perturbation theory in one-loop order in Ref. [15]. A non-perturbatively determination is not yet available. For the renormalization in the continuum theory, we

adopt the modified minimal subtraction scheme ( $\overline{\text{MS}}$ ) with naive dimensional regularization scheme (NDR). We choose two values  $q^* = 1/a$  and  $\pi/a$  as the matching scale from the lattice to the continuum theory in order to estimate the systematic error coming from higher orders of perturbation theory. Large tadpole contributions in the renormalization factors for the lattice perturbation theory are subtracted by the mean-field improvement. We use a mean-field improved value in the  $\overline{\text{MS}}$  scheme for the coupling constant, which is given from the bare coupling constant  $g^2$  by

$$1/g_{\overline{\text{MS}}}^2(q^*) = (C_0 P + 8C_1 R)/g^2 - 0.1006 + 0.03149 \cdot N_f + (11 - 2N_f/3)/(8\pi^2) \cdot \log(q^* a) \quad (97)$$

for our gluon and fermion actions, where  $C_0 = 1 - 8C_1$  and  $C_1 = -0.331$  are the parameters in the gluon action, and  $P$  is the expectation value of the plaquette and  $R$  is that of the  $1 \times 2$  Wilson loop. The detail of the procedure was discussed in Ref. [17]. From the values  $P = 0.572059(31)$  and  $R = 0.338902(47)$  given in Ref. [10], we obtain  $g_{\overline{\text{MS}}}^2 = 2.699$  at  $q^* = 1/a$  and  $g_{\overline{\text{MS}}}^2 = 1.996$  at  $q^* = \pi/a$ .

The decay amplitudes  $A_I$  ( $I = 0, 2$ ) are calculated from (1) as

$$A_I = \sum_{i,j=1}^{10} \overline{M}_i^I(q^*) U_{ij}(q^*, \mu) C_j(\mu) , \quad (98)$$

where

$$C_i(\mu) = \frac{G_F}{\sqrt{2}} (V_{us}^* V_{ud}) (z_i(\mu) + \tau y_i(\mu)) . \quad (99)$$

The explicit form of the functions  $z_i(\mu)$  and  $y_i(\mu)$  in the NDR scheme have been given in Ref. [12]. The functions  $U_{ij}(q^*, \mu)$  are the running factor of the operators  $Q_i$  from the scale  $q^*$  to  $\mu$  for the number of active quark flavors equal to  $N_f = 3$ , which have also been given in Ref. [12]. In the present work we set  $\mu = m_c = 1.3 \text{ GeV}$  in (98) and evaluate the two functions  $z_i(\mu)$  and  $y_i(\mu)$  with the Standard Model parameters tabulated in Table III. We adopt the standard representation of the CKM matrix, in which  $CP$  violation enters entirely through the complex phase of  $V_{td}$ , thus  $\tau = -(V_{ts}^* V_{td}) / (V_{us}^* V_{ud})$ . The values of the two functions are tabulated in Table IV.

From (96) and (98) the decay amplitudes can be written in terms of the bare matrix element  $M_i^I$  as

$$A_I = \sum_{i=1}^{10} M_i^I \overline{C}_i = \sum_{i=1}^{10} A_I(i) , \quad (A_I(i) = M_i^I \overline{C}_i) , \quad (100)$$

where

$$\overline{C}_i = \sum_{j,k=1}^{10} Z_{ij}(q^* a) U_{jk}(q^*, \mu) C_k(\mu) . \quad (101)$$

The constant  $\overline{C}_i$  should be independent of  $\mu$  and  $q^*$ , and depend only on the lattice cutoff  $1/a$ , if we work in the full order of perturbation theory. We define  $\overline{z}_i$  and  $\overline{y}_i$  by (99) for

$\overline{C}_i$ . The values of these quantities for  $q^* = 1/a$  and  $\pi/a$  at  $\mu = m_c = 1.3 \text{ GeV}$  are given in Table IV.

Our final results of the decay amplitudes are given in Table V. The direct  $CP$  violation parameter  $\epsilon'/\epsilon$  is obtained by

$$\text{Re}(\epsilon'/\epsilon) = \frac{\omega}{\sqrt{2}|\epsilon|} \left( \frac{\text{Im}A_2}{\text{Re}A_2} - \frac{\text{Im}A_0}{\text{Re}A_0} \right), \quad (102)$$

with  $\omega = \text{Re}A_2/\text{Re}A_0$ , where the experimental value of the indirect  $CP$  violation parameter  $|\epsilon| = 2.228 \times 10^{-3}$  is used in the estimation. The statistical errors are estimated by the jackknife procedure with a bin size of 10 configurations (250 MD time units). We also list the results by the RBC-UKQCD Collaboration at  $m_\pi = 422 \text{ MeV}$  [3],  $330 \text{ MeV}$  [4], the physical quark mass in the continuum limit (only for the  $\Delta I = 3/2$  process) [2], and the experimental values for comparison.

From Table V we learn that the dependence on  $q^*$  is negligible for most of the decay amplitudes, but it is very large for  $\text{Im}A_2$ . A non-perturbative determination of the renormalization factor is necessary to obtain a reliable result for this value. We find a large enhancement of the  $\Delta I = 1/2$  process over that for the  $\Delta I = 3/2$ . The RBC-UKQCD collaboration found that the enhancement was explained as following numerical mechanism [18]. A large cancellation between two dominant quark diagrams occurs for the  $\Delta I = 3/2$  process and it makes  $\text{Re}A_2$  a small value, while this cancellation does not occur for the  $\Delta I = 1/2$  process. We confirm that their explanation is also valid in our case.

Our result for  $A_0$ , particularly for the imaginary part, still has a large statistical error so that we do not obtain a non-zero result for  $\text{Re}(\epsilon'/\epsilon)$  over the error. We observe that the results for  $A_0$  by the RBC-UKQCD Collaboration at a similar pion mass  $m_\pi = 330 \text{ MeV}$  [4] have smaller errors than ours. This is because they use a different two-pion operator for which the wall sources for the two pions are separated by  $\delta = 4$  in the time direction, and they set the fitting range closer to the two-pion source than our case in extracting the matrix elements from the time correlation functions. Improving statistics by devising a more efficient operator for the two-pion state is an important work reserved for the future.

The contributions of the bare matrix element  $M_i^I$  to the decay amplitude  $A_I$  ( $A_I(i)$  in (100)) are tabulated in Table I for the  $\Delta I = 3/2$  and in Table II for the  $\Delta I = 1/2$  process. We find that the main contribution to  $\text{Re}A_2$  comes from the operator  $Q_1$  and  $Q_2$ , and that to  $\text{Im}A_2$  from  $Q_8$ . The main contribution to  $\text{Re}A_0$  comes from the operator  $Q_2$  and that to  $\text{Im}A_0$  from  $Q_6$ .

## V. CONCLUSIONS

In the present work we have reported on our results for the  $K \rightarrow \pi\pi$  decay amplitudes for both the  $\Delta I = 1/2$  and  $3/2$  channels with the Wilson fermion action. We have found that the stochastic method with the hopping parameter expansion technique and the truncated solver method are very efficient for variance reduction, yielding a first result for the  $I = 0$  amplitude with the Wilson fermion action.

We have been able to show a large enhancement of the  $\Delta I = 1/2$  process over that for the  $\Delta I = 3/2$ . However, our result for  $A_0$ , particularly for the imaginary part, still has a large statistical error so that we do not obtain a non-zero result for  $\text{Re}(\epsilon'/\epsilon)$  over the error. Improving statistics by devising a more efficient operator for the two-pion state is an important work reserved for the future.

Our calculation is carried out away from the physical quark masses, and the decay of the  $K$  meson to two zero momentum pions is considered. Calculations at smaller quark masses with physical kinematics, where the two pions in the final state carry finite momentum, is our next step.

### **Acknowledgments**

This research used computational resources of the K computer provided by the RIKEN Advanced Institute for Computational Science and T2K-TSUKUBA by University of Tsukuba through the HPCI System Research Project (Project ID:hp120153). SR16000 at University of Tokyo is also used. This work is supported in part by Grants-in-Aid of the Ministry of Education No. 23340054 and Interdisciplinary Computational Science Program in CCS, University of Tsukuba.

- 
- [1] T. Blum *et al.* (RBC and UKQCD Collaborations), Phys. Rev. Lett. **108**, 141601 (2012) [arXiv:1111.1699]; Phys. Rev. **D86**, 074513 (2012) [arXiv:1206.5142].
  - [2] T. Blum *et al.* (RBC and UKQCD Collaborations), Phys. Rev. **D91**, 074502 (2015) [arXiv:1502.00263].
  - [3] T. Blum *et al.* (RBC and UKQCD Collaborations), Phys. Rev. **D84**, 114503 (2011) [arXiv:1106.2714].
  - [4] Q. Liu (RBC and UKQCD Collaborations), PoS (Lattice 2011)(2011)287 [arXiv:1110.2143].
  - [5] C. Kelly and D. Zhang (RBC and UKQCD Collaborations), PoS (Lattice 2014)(2014)365; D. Zhang and C. Kelly (RBC and UKQCD Collaborations), PoS (Lattice 2014)(2014)366.
  - [6] C.W. Bernard, T. Draper, G. Hockney, A. Soni, Nucl. Phys. Proc. Suppl. 4, 483 (1988).
  - [7] A. Donini, V. Giménez, G. Martinelli, M. Talevi, A. Vladikas, Eur. Phys. J. **C10**, 121 (1999) [arXiv:hep-lat/9902030].
  - [8] C.W. Bernard, T. Draper, A. Soni, H.D. Politzer, M.B. Wise, Phys. Rev. **D32**, 2343 (1985); C. Dawson, G. Martinelli, G.C. Rossi, C.T. Sachrajda, S. Sharpe, M. Talevi, M. Testa, Nucl. Phys. **B514**, 313 (1998) [arXiv:hep-lat/9707009].
  - [9] L. Maiani, G. Martinelli, G. Rossi, M. Testa, Nucl. Phys. **B289**, 505 (1987); M. Testa, Nucl. Phys. Proc. Suppl. 63, 38 (1998) [arXiv:hep-lat/9709044].
  - [10] S. Aoki *et al.* (PACS-CS Collaboration), Phys. Rev. **D79**, 034503 (2009) [arXiv:0807.1661].
  - [11] N. Ishizuka, K.-I. Ishikawa, A. Ukawa, T. Yoshié, PoS (Lattice 2013)(2013)474 [arXiv:1311.0958]; PoS (Lattice 2014)(2014)364 [arXiv:1410.8237].
  - [12] For a review, see, G. Buchalla, A.J. Buras, M.E. Lautenbacher, Rev. Mod. Phys. 68, 1125 (1996).
  - [13] G.S. Bali, S. Collins, A. Schäfer, Comput. Phys. Commun. **181**, 1570 (2010) [arXiv:0910.3970].
  - [14] L. Lellouch and M. Lüscher, Commun. Math. Phys. **219**, 31 (2001) [arXiv:hep-lat/0003023].
  - [15] Y. Taniguchi, JHEP 04 (2012) 143 [arXiv:1203.1401].
  - [16] J. Beringer *et al.* (Particle Data Group), Phys. Rev. **D 86**, 010001 (2012).
  - [17] A. Ali Khan *et al.* (CP-PACS Collaboration), Phys. Rev. **D65**, 054505 (2002) [arXiv:hep-lat/010515]; Phys. Rev. **D67**, 059901 (2003).
  - [18] P.A. Boyle *et al.* (RBC and UKQCD Collaborations), Phys. Rev. Lett. **110**, 152001 (2013) [arXiv:1212.1474].

# Figures

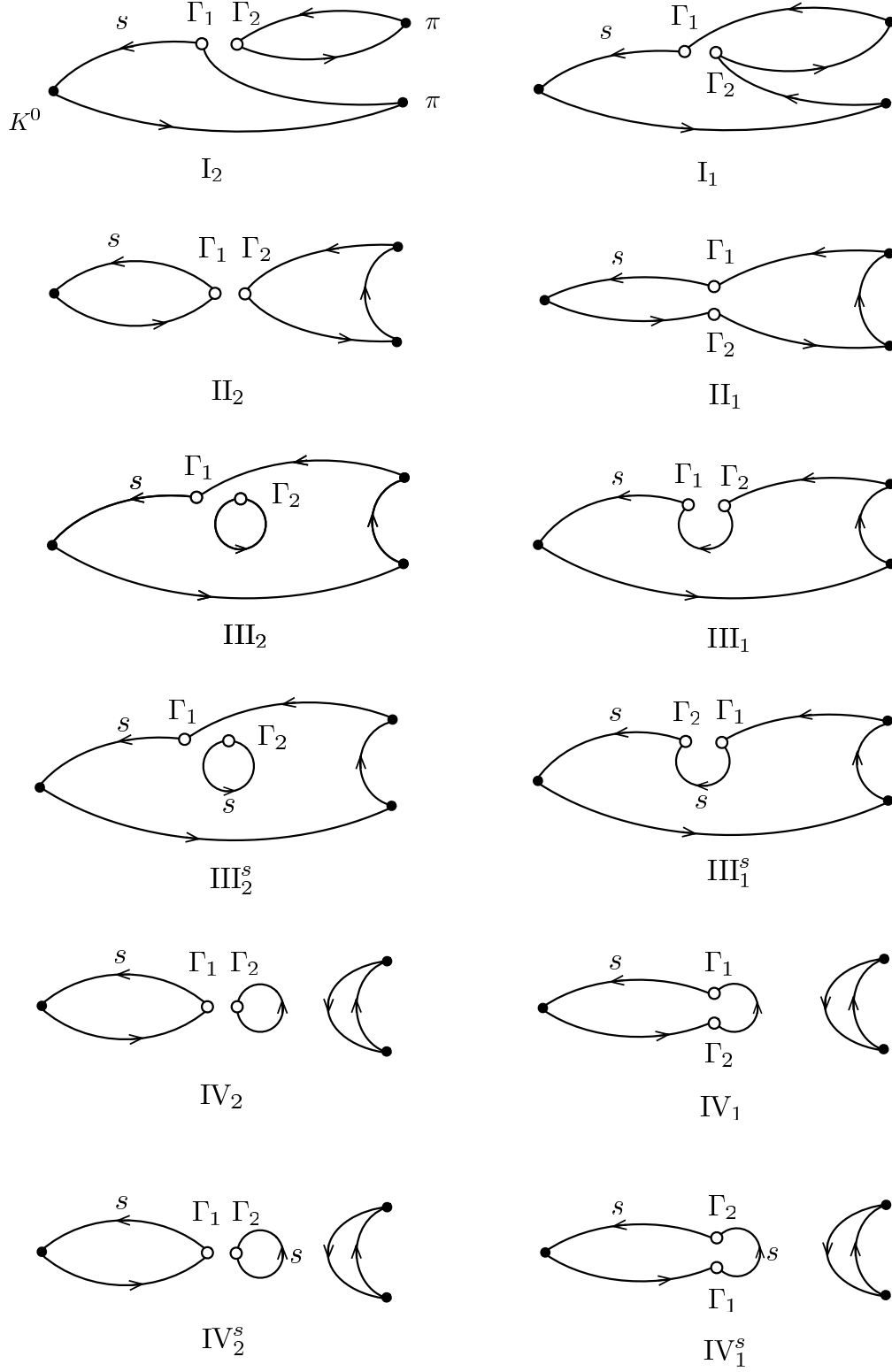


FIG. 1: Quark contractions for the time correlation function for the  $K \rightarrow \pi\pi$  process for the operator  $Q_i$  ( $i = 1, 2, \dots, 10$ ).

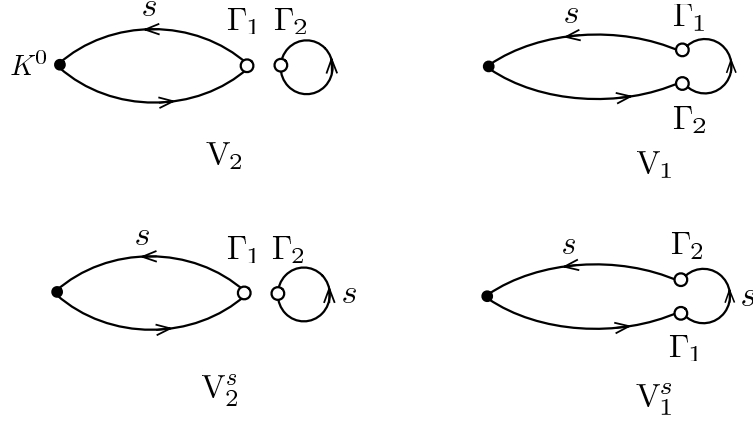


FIG. 2: Quark contractions for the time correlation function for the  $K \rightarrow 0$  process for the operator  $Q_i$  ( $i = 1, 2, \dots, 10$ ).

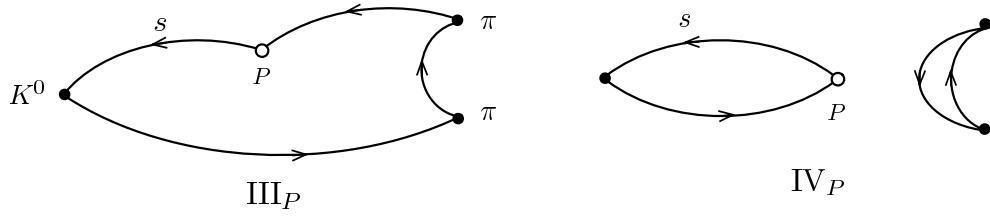


FIG. 3: Quark contractions for the time correlation function for the  $K \rightarrow \pi\pi$  process for the operator  $P = \bar{s}\gamma_5 d$ .

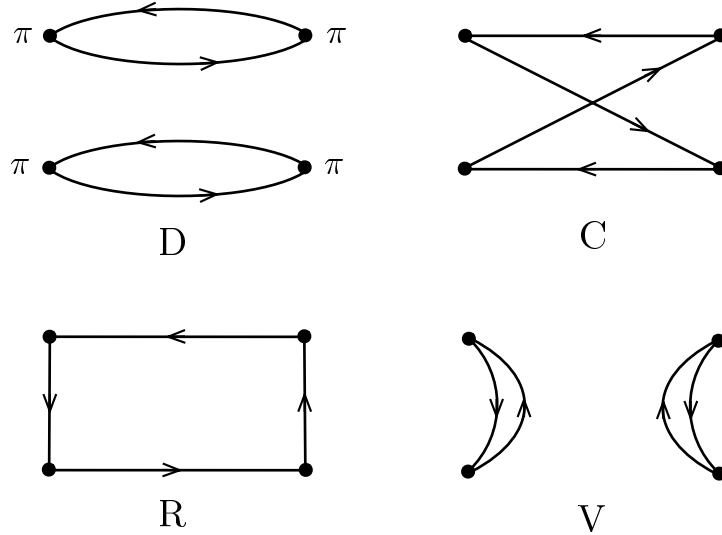


FIG. 4: Quark contractions for the time correlation function for  $\pi\pi \rightarrow \pi\pi$ .



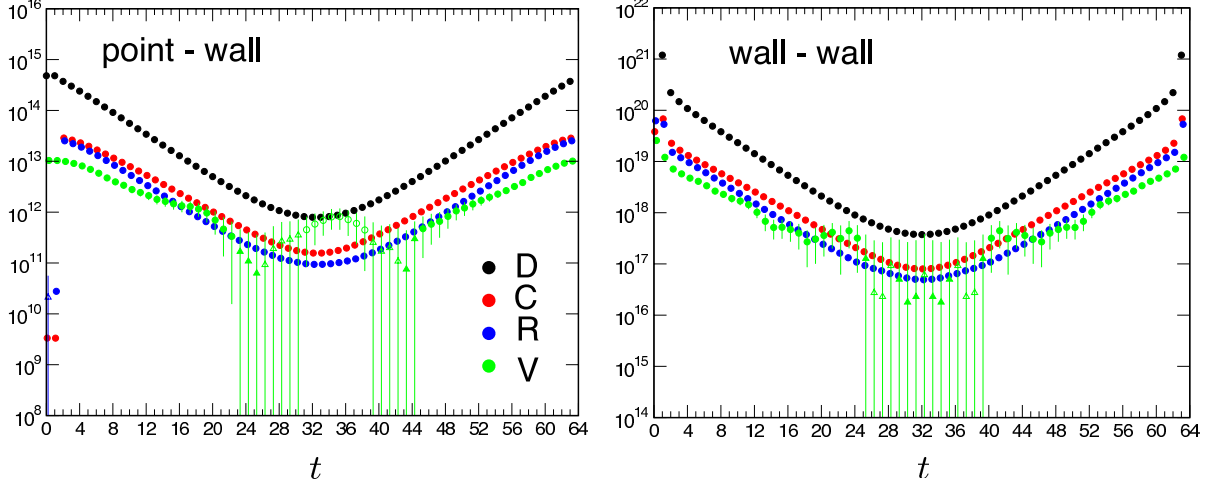


FIG. 5: Fore types of contractions for the time correlation function for  $\pi\pi \rightarrow \pi\pi$ . Left panel shows those for the point-wall function  $G_{PW}^I(t)$  in (73) and right for the wall-wall function  $G_{WW}^I(t)$  in (74).

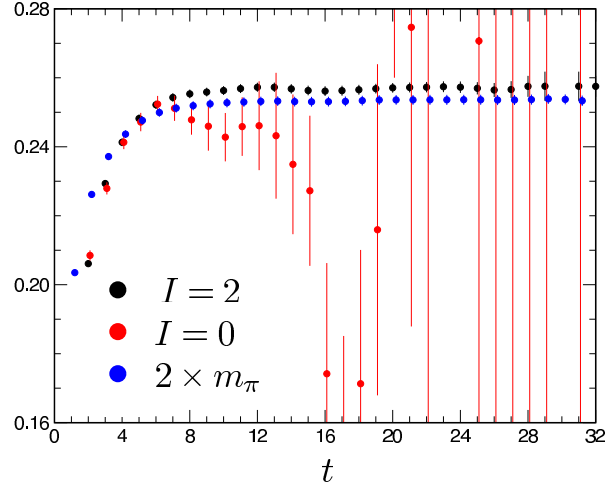


FIG. 6: Effective mass of the time correlation function  $G_{PW}^I(t)$  for  $\pi\pi \rightarrow \pi\pi$  with the iso-spin  $I = 0$  and  $I = 2$ . Twice of the effective mass for the pion is also plotted for a comparison.

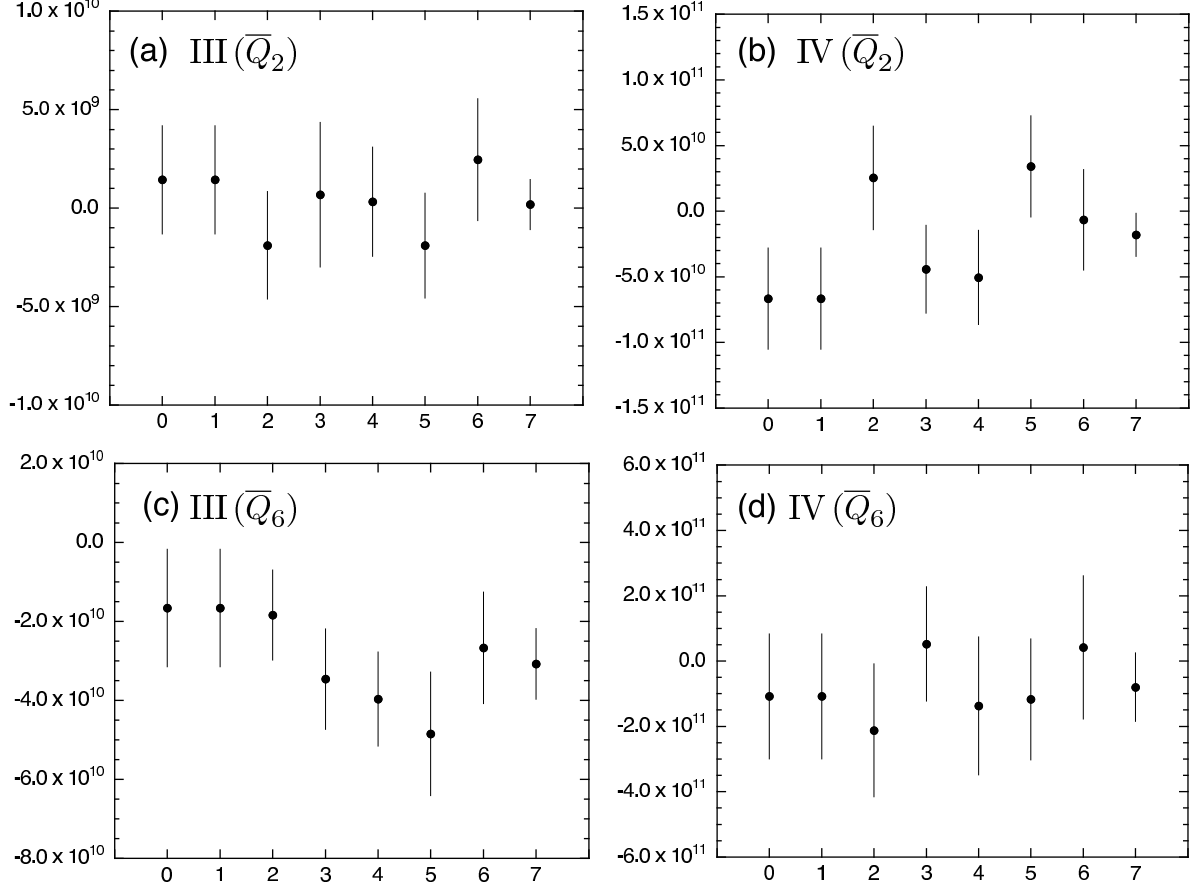


FIG. 7: Effect of the truncated solver method. Panels (a)-(d) show the contributions of the contraction III and IV to the time correlation functions for  $\overline{Q}_2$  and  $\overline{Q}_6$  at  $t = 9$ . In each panel, the data at  $x = 0$  show the contribution obtained by the usual stochastic method (69) with  $N_R = 1$ , *i.e.*, the contribution given by setting the quark loop  $Q(\mathbf{x}, t; \mathbf{x}, t) = \xi_i^*(\mathbf{x}, t) S_i(\mathbf{x}, t)$  for  $i = 1$ . The data at  $x = 1, 2, \dots, 6$  correspond to the contributions given by setting  $Q(\mathbf{x}, t; \mathbf{x}, t) = \xi_i^*(\mathbf{x}, t) S_i^T(\mathbf{x}, t)$  for  $x = i = 1, 2, \dots, 6$  ( $N_R + N_T = 1 + 5$ ) with  $S_i^T(\mathbf{x}, t)$  in (72). The data at  $x = 7$  are average of the data at  $x = 1, 2, \dots, 6$ .

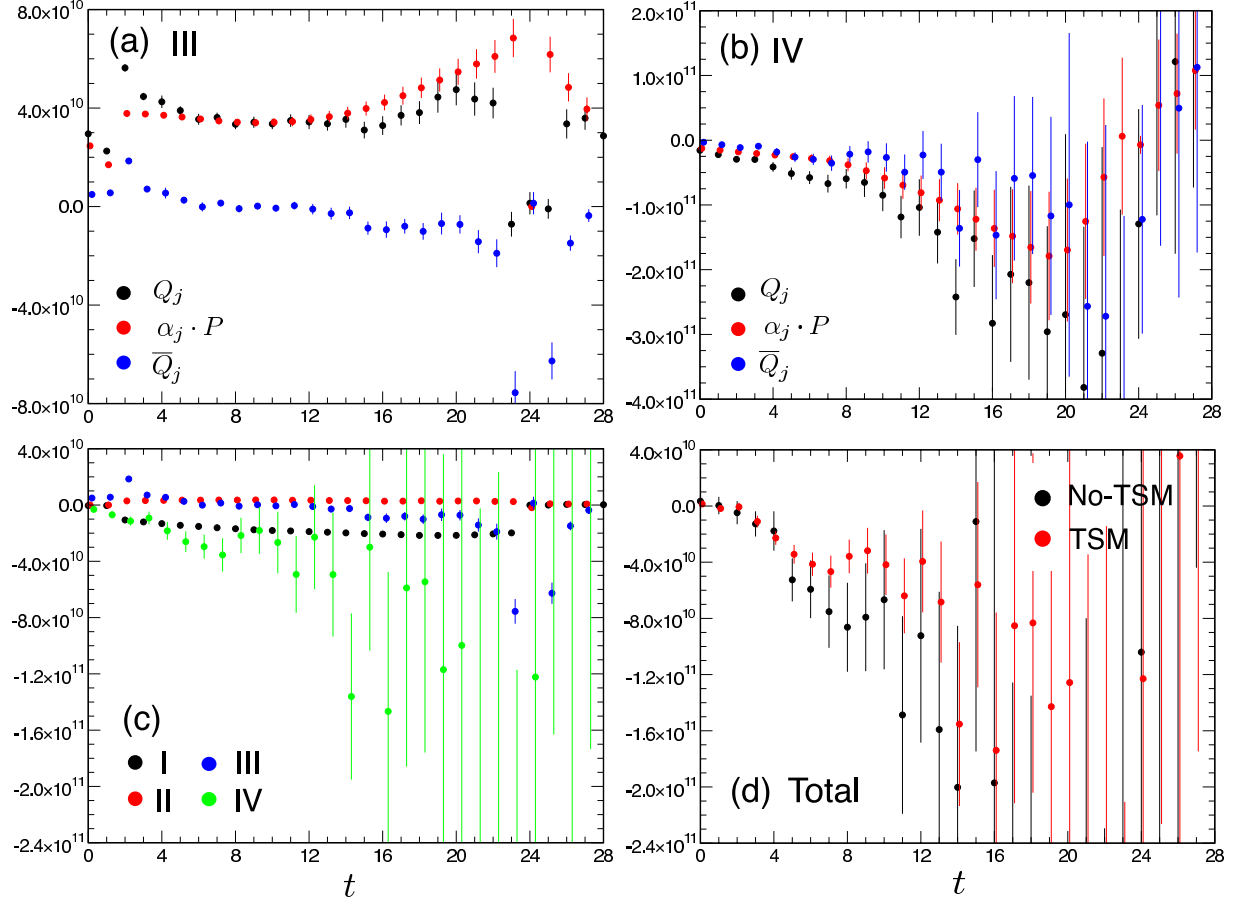


FIG. 8: Time correlation function for the operator  $Q_2$  for the  $\Delta I = 1/2$   $K \rightarrow \pi\pi$  process,  $G_2^{I=0}(t)$  in (25). The time slices of the two-pion and the  $K$  meson are set at  $t_\pi = 0$  and  $t_K = 24$ , while the operator  $Q_i$  runs over the whole time extent. (a) Contributions of the contraction III for  $Q_2$ ,  $\alpha_2 \cdot P$  and  $\bar{Q}_2 = Q_2 - \alpha_2 \cdot P$ . (b) Contributions of the contraction IV for  $Q_2$ ,  $\alpha_2 \cdot P$  and  $\bar{Q}_2 = Q_2 - \alpha_2 \cdot P$ . (c) Contributions from each type of contractions for  $\bar{Q}_2$ , (d) Total correlation functions calculated with TSM and without TSM.

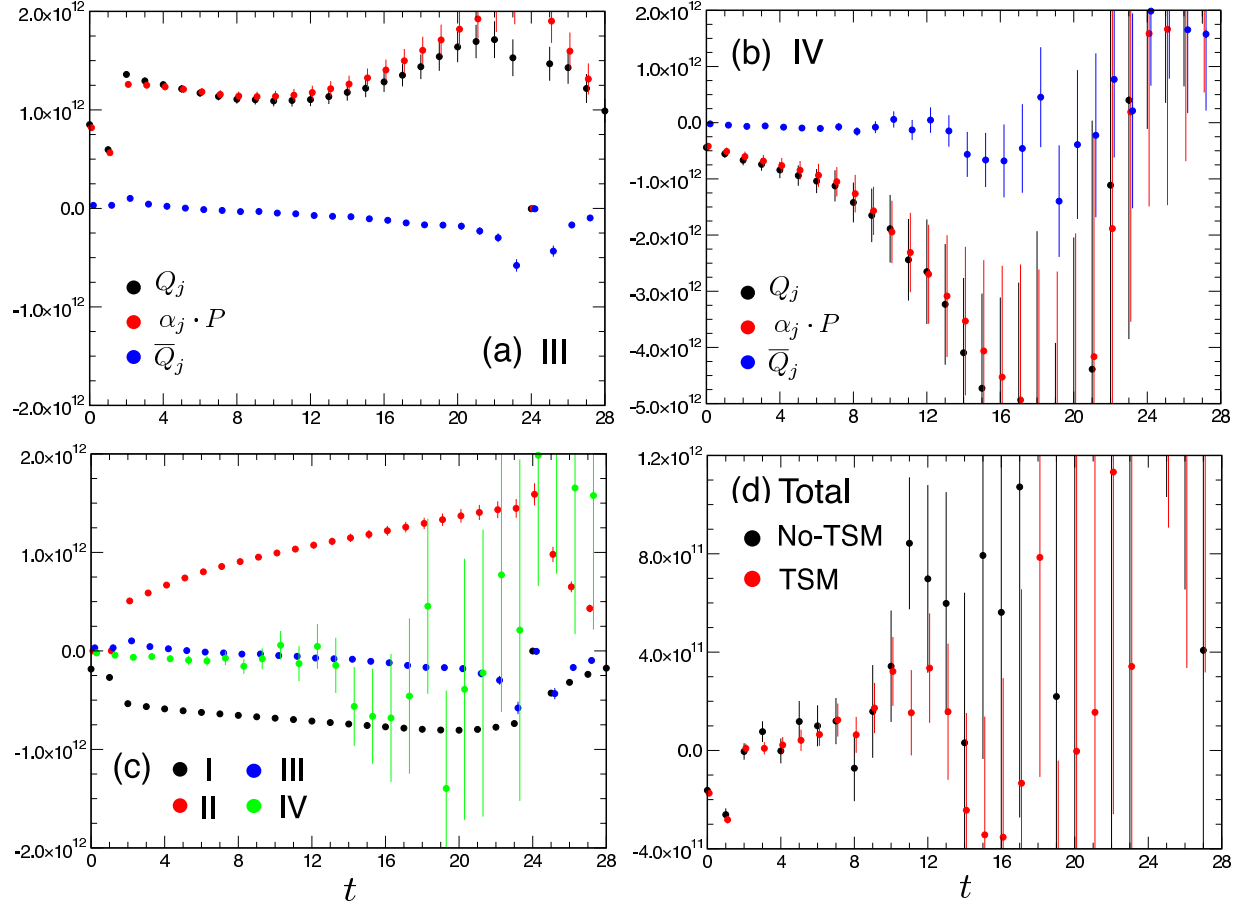


FIG. 9: Time correlation function for the operator  $Q_6$  for the  $\Delta I = 1/2$   $K \rightarrow \pi\pi$  process,  $G_6^{I=0}(t)$  in (25), following the same convention as in Fig. 8.

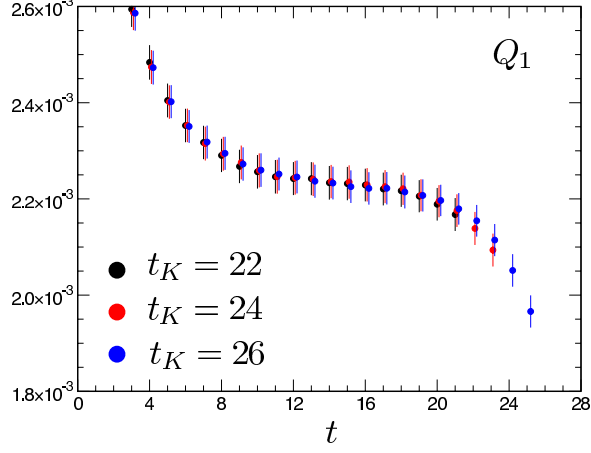


FIG. 10: Effective matrix element of  $M_1^{I=2}(t)$  in (92), in the lattice unit. The time slice of the two-pion is set at  $t_\pi = 0$ . The operator  $Q_i(t)$  runs over the whole time extent. The matrix elements given with the  $K$  meson at time slice  $t_K = 22, 24, 26$  are plotted.

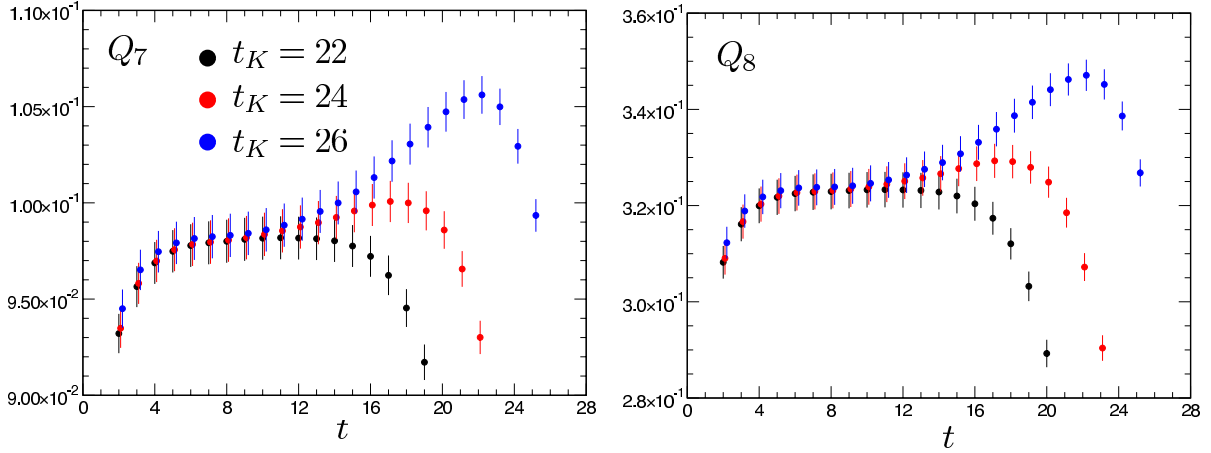


FIG. 11: Effective matrix elements of  $M_{7,8}^{I=2}(t)$  in (92), following the same convention as in Fig. 10.

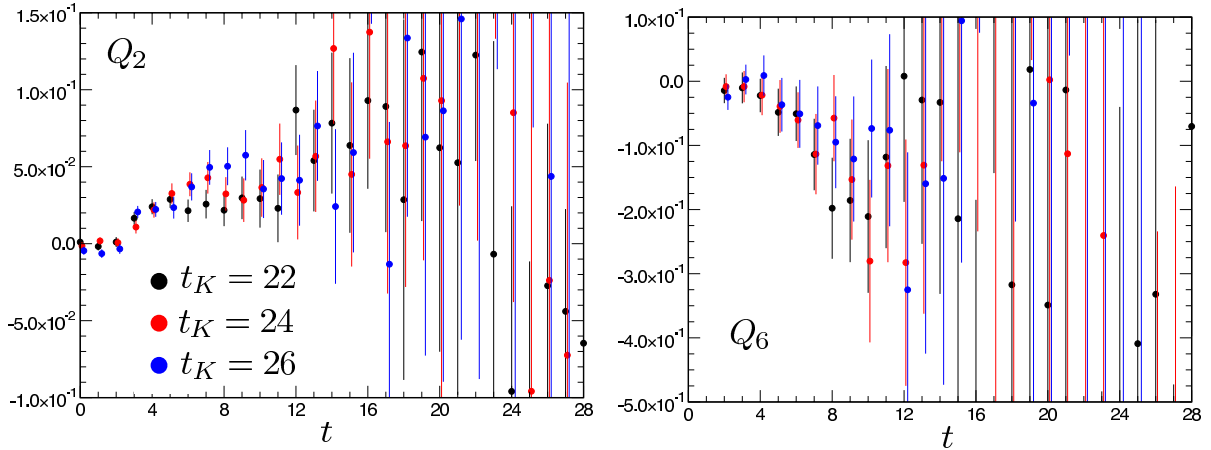


FIG. 12: Effective matrix elements of  $M_{2,6}^{I=0}(t)$  in (92), following the same convention as in Fig. 10.

## Tables

TABLE I: Decay amplitude for the  $\Delta I = 3/2$  process. The second column gives the bare matrix elements  $M_i^{I=2}$  for  $Q_i$  in the lattice unit. The other columns are their contribution to  $A_2$  (  $A_2(i)$  in (100) ) for  $q^* = 1/a$  and  $\pi/a$ .

$i$	$M_i^I$	$q^* = 1/a$		$q^* = \pi/a$	
		$\text{Re}A_2 \text{ (GeV)}$	$\text{Im}A_2 \text{ (GeV)}$	$\text{Re}A_2 \text{ (GeV)}$	$\text{Im}A_2 \text{ (GeV)}$
1	$2.256(35) \times 10^{-3}$	$-1.887(29) \times 10^{-08}$	0	$-1.452(23) \times 10^{-08}$	0
2	$= M_1^{I=2}$	$4.330(68) \times 10^{-08}$	0	$3.920(61) \times 10^{-08}$	0
7	$9.85(11) \times 10^{-2}$	$1.053(12) \times 10^{-10}$	$2.772(32) \times 10^{-13}$	$3.172(36) \times 10^{-10}$	$2.100(24) \times 10^{-13}$
8	$3.242(37) \times 10^{-1}$	$-2.722(31) \times 10^{-10}$	$-1.670(19) \times 10^{-12}$	$-4.124(47) \times 10^{-10}$	$-1.156(13) \times 10^{-12}$
9	$= 3/2 \cdot M_1^{I=2}$	$-1.140(18) \times 10^{-12}$	$3.762(59) \times 10^{-13}$	$3.739(58) \times 10^{-12}$	$3.409(53) \times 10^{-13}$
10	$= 3/2 \cdot M_1^{I=2}$	$3.771(59) \times 10^{-10}$	$-1.756(27) \times 10^{-13}$	$4.372(68) \times 10^{-10}$	$-1.409(22) \times 10^{-13}$
Total	-	$2.426(38) \times 10^{-08}$	$-1.192(14) \times 10^{-12}$	$2.460(38) \times 10^{-08}$	$-7.457(83) \times 10^{-13}$

TABLE II: Decay amplitude for the  $\Delta I = 1/2$  process. The second column gives the bare matrix elements  $M_i^{I=0}$  for  $Q_i$  in the lattice unit. The other columns are their contribution to  $A_0$  (  $A_0(i)$  in (100) ) for  $q^* = 1/a$  and  $\pi/a$ .

$i$	$M_i^I$	$q^* = 1/a$		$q^* = \pi/a$	
		$\text{Re}A_0 \text{ (GeV)}$	$\text{Im}A_0 \text{ (GeV)}$	$\text{Re}A_0 \text{ (GeV)}$	$\text{Im}A_0 \text{ (GeV)}$
1	$0.5(1.3) \times 10^{-2}$	$-0.4(1.1) \times 10^{-07}$	0	$-3.1(8.5) \times 10^{-08}$	0
2	$3.6(1.4) \times 10^{-2}$	$6.8(2.8) \times 10^{-07}$	0	$6.2(2.5) \times 10^{-07}$	0
3	$7.2(3.7) \times 10^{-2}$	$-1.25(65) \times 10^{-08}$	$-2.5(1.3) \times 10^{-11}$	$-1.7(8.7) \times 10^{-08}$	$-2.1(1.1) \times 10^{-11}$
4	$1.06(40) \times 10^{-1}$	$5.3(2.0) \times 10^{-08}$	$6.6(2.5) \times 10^{-11}$	$6.2(2.4) \times 10^{-08}$	$6.1(2.3) \times 10^{-11}$
5	$-1.0(4.3) \times 10^{-2}$	$1.5(5.9) \times 10^{-09}$	$1.7(6.8) \times 10^{-12}$	$1.9(7.4) \times 10^{-09}$	$1.8(7.1) \times 10^{-12}$
6	$-2.0(1.1) \times 10^{-1}$	$-8.4(4.6) \times 10^{-08}$	$-1.03(56) \times 10^{-10}$	$-7.7(4.2) \times 10^{-08}$	$-8.8(4.8) \times 10^{-11}$
7	$2.42(18) \times 10^{-1}$	$2.58(19) \times 10^{-10}$	$6.81(50) \times 10^{-13}$	$7.79(57) \times 10^{-10}$	$5.16(38) \times 10^{-13}$
8	$7.46(54) \times 10^{-1}$	$-6.26(45) \times 10^{-10}$	$-3.84(28) \times 10^{-12}$	$-9.48(68) \times 10^{-10}$	$-2.66(19) \times 10^{-12}$
9	$-3.0(1.4) \times 10^{-2}$	$1.02(48) \times 10^{-11}$	$-3.4(1.6) \times 10^{-12}$	$-3.4(1.6) \times 10^{-11}$	$-3.1(1.4) \times 10^{-12}$
10	$0.0(1.2) \times 10^{-2}$	$0.0(1.4) \times 10^{-11}$	$-0.1(6.4) \times 10^{-13}$	$0.0(1.6) \times 10^{-11}$	$-0.1(5.2) \times 10^{-13}$
Total	-	$6.0(3.6) \times 10^{-07}$	$-6.7(5.6) \times 10^{-11}$	$5.6(3.2) \times 10^{-07}$	$-5.2(4.8) \times 10^{-11}$

TABLE III: Standard model parameters used to evaluate the decay amplitudes in the present work (from Ref. [16]).  $\tau = -(V_{ts}^* V_{td}) / (V_{us}^* V_{ud})$  and  $\Lambda_{\overline{\text{MS}}}^{(5)}$  is the lambda QCD for  $N_f = 5$  theory. The standard representation of the CKM matrix of Ref. [16] is adopted, where the  $CP$  violation enters entirely through a complex phase of  $V_{td}$ , thus  $\tau$ .

$m_Z$	91.188 GeV
$m_W$	80.385 GeV
$m_t$	173 GeV
$m_b$	4.2 GeV
$m_c$	1.3 GeV
$\Lambda_{\overline{\text{MS}}}^{(5)}$	0.23135 GeV
$\alpha$ ( at $\mu = m_W$ )	1/129
$\sin^2 \theta_W$	0.230
$G_F$	$1.166 \times 10^{-5} \text{ GeV}^{-2}$
$V_{ud}$	0.97427
$V_{us}$	0.22534
$\text{Re}(\tau)$	0.001513
$\text{Im}(\tau)$	-0.000601

TABLE IV:  $z_i(\mu)$ ,  $y_i(\mu)$ ,  $\bar{z}_i$  and  $\bar{y}_i$ . The parameters of the standard model tabulated in Table III are used in the calculations. We set  $\mu = m_c = 1.3 \text{ GeV}$ , and choose two values  $q^* = 1/a$  and  $\pi/a$  as the matching scale from the lattice to the continuum.

$i$			$q^* = 1/a$		$q^* = \pi/a$	
			$\bar{z}_i$	$\bar{y}_i$	$\bar{z}_i$	$\bar{y}_i$
1	$-4.184 \times 10^{-1}$	0	$-4.487 \times 10^{-1}$	0	$-3.453 \times 10^{-1}$	0
2	$1.218 \times 10^{+0}$	0	$1.029 \times 10^{+0}$	0	$9.321 \times 10^{-1}$	0
3	$4.575 \times 10^{-3}$	$2.910 \times 10^{-2}$	$-9.327 \times 10^{-3}$	$3.145 \times 10^{-2}$	$-1.246 \times 10^{-2}$	$2.629 \times 10^{-2}$
4	$-1.373 \times 10^{-2}$	$-5.782 \times 10^{-2}$	$2.703 \times 10^{-2}$	$-5.628 \times 10^{-2}$	$3.173 \times 10^{-2}$	$-5.108 \times 10^{-2}$
5	$4.575 \times 10^{-3}$	$4.869 \times 10^{-3}$	$-7.309 \times 10^{-3}$	$1.402 \times 10^{-2}$	$-9.284 \times 10^{-3}$	$1.470 \times 10^{-2}$
6	$-1.373 \times 10^{-2}$	$-9.009 \times 10^{-2}$	$2.323 \times 10^{-2}$	$-4.700 \times 10^{-2}$	$2.130 \times 10^{-2}$	$-4.015 \times 10^{-2}$
7	$6.305 \times 10^{-5}$	$-2.010 \times 10^{-4}$	$5.777 \times 10^{-5}$	$-2.514 \times 10^{-4}$	$1.731 \times 10^{-4}$	$-1.904 \times 10^{-4}$
8	0	$1.098 \times 10^{-3}$	$-4.573 \times 10^{-5}$	$4.600 \times 10^{-4}$	$-6.871 \times 10^{-5}$	$3.183 \times 10^{-4}$
9	$6.305 \times 10^{-5}$	$-1.168 \times 10^{-2}$	$-3.047 \times 10^{-6}$	$-9.925 \times 10^{-3}$	$7.287 \times 10^{-5}$	$-8.995 \times 10^{-3}$
10	0	$4.357 \times 10^{-3}$	$5.277 \times 10^{-5}$	$4.635 \times 10^{-3}$	$6.368 \times 10^{-5}$	$3.717 \times 10^{-3}$

TABLE V: Results of the  $K \rightarrow \pi\pi$  decay amplitudes. The results by the RBC-UKQCD Collaboration at  $m_\pi = 422 \text{ MeV}$  [3],  $330 \text{ MeV}$  [4], the physical quark mass in the continuum limit (only for the  $\Delta I = 3/2$  process) [2], and the experimental values are also tabulated for comparison.

	$q^* = 1/a$	$q^* = \pi/a$	RBC-UKQCD			Exp.
$a \text{ (fm)}$	0.091		0.114	0.114	-	-
$m_\pi \text{ (MeV)}$	280		330	422	140	140
$\text{Re}A_2 (\times 10^{-8} \text{ GeV})$	2.426(38)	2.460(38)	2.668(14)	4.911(31)	1.50(4)(14)	1.479(4)
$\text{Re}A_0 (\times 10^{-8} \text{ GeV})$	60(36)	56(32)	31.1(4.5)	38.0(8.2)		33.2(2)
$\text{Re}A_0/\text{Re}A_2$	25(15)	23(13)	12.0(1.7)	7.7(1.7)		22.45(6)
$\text{Im}A_2 (\times 10^{-12} \text{ GeV})$	-1.192(14)	-0.7457(83)	-0.6509(34)	-0.5502(40)	-0.699(20)(84)	
$\text{Im}A_0 (\times 10^{-12} \text{ GeV})$	-67(56)	-52(48)	-33(15)	-25(22)		
$\text{Re}(\epsilon'/\epsilon)(\times 10^{-3})$	0.8(2.5)	0.9(2.5)	2.0(1.7)	2.7(2.6)		1.66(23)